UNIVERSITY OF CALIFORNIA,
IRVINE

Optimal Design, Dispatch, and Reliable Operation of Alternative Energy Sources and Storage Systems in Microgrids

THESIS

submitted in partial satisfaction of the requirements
for the degree of

MASTER OF SCIENCE

in Electrical and Computer Engineering

by

Weixi Wang

Thesis Committee:
Professor Jack Brouwer, Co-Chair
Professor Pramod Khargonekar, Co-Chair
Professor Keyue Smedley

2022

Table of Contents

Table of Figures

Table of Tables

Acknowledgements

I would like to express my sincerest and deepest gratitude to Professor Jack Brouwer for serving as my advisor and thesis committee chair. His professional guidance and expertise have inspired me to work creatively and see though the appearance of questions to the essence. This thesis would not have completed without his constant support. I am also extremely grateful to him for accepting me and giving me the opportunity to join the Advanced Power and Energy Program (APEP).

I would also like to sincerely thank Professor Pramod Khargonekar for serving as my co-advisor and thesis chair, whose work on Machine Learning has motivated me and provided a different angle in problem-solving.

I am also very grateful for Professor Keyue Smedley for serving on my thesis committee and for bringing insights into the fundamentals of electric devices.

I would also like to extend my thank to Dr. Robert Flores for his patient help on my study and analysis and for all the weekly meetings and time. I would also like to thank Dr. Laura Novoa, Dr. Ghazal Razeghi as well as Dr. Jennifer Lee for their help and support.

In addition, a thank you to all my family and friends as well as all the APEP members

for all their support they have provided during my study.

I would like to acknowledge the financial support for my research, which was provided by the California Energy Commission, contract number: EPC-17-045.

Abstract of the Thesis

Optimal Design, Dispatch, and Reliable Operation of Alternative Energy Sources and Storage Systems in Microgrids

by

Weixi Wang

Master of Science in Electrical Engineering

University of California, Irvine, 2022

Professor Jack Brouwer, Co-Chair

Professor Pramod Khargonekar, Co-Chair

An increase in people's awareness of climate change and its ensuing consequence of increased power failures have given rise to discussions on ways to enhance energy reliability, which includes transitioning to microgrid. With the vast majority of grid system still being conventional, it is more practical to build microgrids based on existing ones. This thesis proposes a specific algorithm to transform existing community scale power grid system to microgrids aiming at enhancing energy reliability and resiliency, and a real-life disadvantaged community is modeled and analyzed upon with added Distributed Energy Resource (DER) and Energy Storage System (ESS). The physical power flow model of the real-life disadvantaged community that is applicable to a mixed residential/commercial/industrial neighborhood was first developed on simulation software OpenDSS. Before applying the baseline load separately generated by DERopt tool, E3 RESOLVE model was used to verify its accuracy. Different levels of electric vehicle (EV) charging load were then estimated and added on top of the baseline community scale energy

model designed to reflect on current trends. A revised multilevel Graph-Partitioning algorithm combined with Mixed-integer linear programming (MILP) was then developed and implemented to optimally separate the existing community grid connections into different islands that yield best possible static balance between local power supply and demand with added DER/ESS. Results shows that under various penetration of EV adoption and DER/ESS our algorithm works to provide the most reliable, resilient energy supply to the community.

1 Introduction

With microgrids gaining increasing popularity throughout the world, reliable operation of microgrids has been a hot research topic in recent years. Originally developed based off centered electric grids, microgrids stand out as a modern solution to fight climate change and greenhouse gas and pollutant emission. Key infrastructures in every microgrid includes Distributed Energy Resources (DERs) and Energy Storage System (ESS), which power and regulate energy usage respectively. Most common DERs today are Solar Energy Systems (SES), or photovoltaic systems (PV), which transforms solar energy to electric energy. One major aim of coupling DERs and ESSs in microgrids is to ensure local power availability whenever the grid system needs to work off center due to possible power failures on centralized power distribution system resulted from ether accident or climate change. While the steady decrease in PV system cost has rendered available a vast residential and commercial installation in recent decades, the unstableness of solar energy due to its mercurial nature has cast doubt on its ability to reliably power the utility customers. An intermittent energy generation system highly affected by whether condition and subject to daylight hours, solar systems not only need to deal with inconsistency and imbalance in energy generation, energy quality that may very well contains harmful high-ordered harmonics is also serious concern [1]. To solve the problem, solutions have been proposed which includes mitigators in solar inverters.

To sufficiently harness the energy produced by PV system without the limitation of sporadicity, ESS was introduced into microgrids. By intentionally regulating the power by charging and discharging at given time, energy storage system stables PV system's power output. One very common strategy that couples PV and ESS is peak shaving and valley

filling, where the ESS mitigate the peak energy usage where electricity price is high by discharging stored energy and instead shifting part of the peak load into hours when energy usage is low and energy price is low accordingly, which is usually evening hours, by charging the battery [2]. While local utility customers enjoy the financial benefit of the strategy by paying less on their energy bills, local energy providers and operators also benefit with a reduced risk of power failure associated with peak energy demand exceeding maximum supply level.

The recent vast adoption of electric vehicles (EV) has also brought new challenges to the operation of microgrids. Propelled by subsidization and tax credit incentives, EVs are getting increasingly popular. However, a high EV penetration rate always results in heavy burden on electric infrastructure, which without proper design, control or even upgrade may result in failure. The different levels of EV chargers and types also means a more complicated than usual electric demand. The socioeconomic level of different areas always translates to differences in ability to adopt EV as well, and an estimate of current or future adoption rate for a given area as well as a way to estimate chargers amount is important. The Vehicle-to-Grid (V2G) technology that considers EV's battery as a distributed energy storage system is also gaining attention, the addition of which is adding up complicity of microgrids as well [3–5].

With all those advantages of microgrids in mind, it is not easy to transition from macro grids to microgrids. While many cities and communities through the world has considered the ideas of microgrids from the start of community development and several have in fact succeeded, most of the power grids is still conventional. Therefore, it is most practical for engineers to design methods to transform existing grids to microgrids. Many designs have been proposed by scientists. While most focus on working out designs based on

specific design requirements, such as [6–8], few have been suggested that applies directly to a general topology.

This thesis contributes to measures to transform existing community scale grid systems into microgrids, and is achieved by:

1. Creating a real-life AC Power Flow model in OpenDSS based on the Oak View Community located in Huntington Beach, California
2. Verifying the accuracy of the AC Power Flow model of the community on DEROPT using E3 RESOLVE tool
3. Estimating and adding different levels of EV charging demand as well as DER penetration and ESS on top of baseline load from DEROPT
4. Developing a topology design model tailored to directly generate islands with existing radially developed cable connections and add switches to optimally balance the power demand and supply within each island
5. Evaluation of performance of microgrids with and without the installation of DER/ESS under both grid connected and islanded operation mode

2 Literature Review

2.1 Power Grid and its Technologies

The power grid plays an import role in contemporary society. Connecting domestic and industrial power needs with power lines, power grids distribute bulk energy sources and consequently have contributed significantly to America's economic growth in the 20thcentury [9]. Therefore, a steady and reliable grid structure must be ensured. Early stage grids can be dated to as far back as the 1880s, when Dolgeville Hydro-power station in New York powered industrial demands [10]. Even though technology advances have brought about significant changes, including AC transmission lines and high-performance transformers, the update and modernization of grid dynamics and overloaded network constraints has been a national concern within the U.S. and a worldwide problem as a whole [11]. To meet national demand, several kinds of technology have been researched, experimented and applied. Since real-life experiments involving dispatch of the grid seem difficult considering the scale, complexity of the network, and implications for end-users, simulation tools are preferred by scientists and researchers to investigate options.

2.2 Solar Energy in the Power Grid

As one of the most considered alternative sources, solar energy systems, most popularly photovoltaic or PV systems, have been evolving throughout the years. It is acknowledged that modern grid systems, especially the high-tech smart grid systems all

around the world, should integrate high levels of PV as renewable energy generators, partly because the need to reduce greenhouse gas emission and to liberate energy markets [12].

Operating steadily on solar radiation, PV solar panels harness solar energy silently. However, PV systems do have limitations and downsides. Apart from energy demands and greenhouse gas and toxic pollution produced during solar cells' manufacturing, energy from PV systems also affect power quality and grid network dynamics. With more PV being incorporated into the macro grids, energy quality problem such as Total Harmonic Distortion (THD) has become a big concern [1]. The uncertainty of generation environment directly leads to the fluctuation of power and harmonics in solar inverters, which must be dealt with before being transmitted into a grid system.

Multiple solutions to solve the THD problem have been proposed by researchers. One way that has already seen limited practical use was developed by T. Ito et al. to reduce the harmonics by deploying a prototype of the power conditioning system (PCS) of a certain power capacity [13]. Apart from that, it has been argued that the resonant current control method and its advanced variants can cope with the THD problem at the cost of computational load increase [14].

PV systems have many applications. One recent design and use of PV in a smart grid system in Brazil has served the role of peak demand reduction [3]. It is argued that the new energy demand deriving from the use of EVs can be met in urbanized areas by PV systems [3]. It is further argued that grid operation cost may be reduced considering the fact that urban electricity price is constrained by demand and peak price is especially high. By reducing the load of feeders during the peak time, the application of PV plus storage may well witness a decrease in power expense [3].

2.3 Electrical Vehicles in the Power Grid

Electrical vehicles (EV) have gained much popularity these days. One of the biggest advantages of the electrical vehicle, be it Plug-in Hybrid Electric Vehicle (PHEV) or fully electric Battery Electric Vehicle (BEV), is that exhaust emissions can be reduced. Executive Order B-16-2012 signed by Governor Brown Jr. has stated that a statewide electrification of transportation be met by 2025 and 1.5 million Zero Emission Vehicles (ZEVs) be on road. Executive Order B-48-18 later reaffirms the former Order and set a new goal of 5 million ZEVs on California road [15].

One significant derivative technologies from EV in the field of the power grid is Vehicle-to-Grid (V2G) technology. Interacting with the power between the vehicles and the grid, V2G technology achieves demand response services for the two platforms [16]. It is argued that a special kind of single-phase PEV charger can support the utility grid network by providing reactive power, meanwhile still successfully functioning as a battery-charger [4]. It is also argued that not only a great percentage decrease on CO_2 emission can be achieved, a bigger amount of wind power can be incorporated into the grid system because of V2G application [17]. It is further demonstrated using experiments that, along with the capability to support distribution load, V2G technology can also provide ancillary services, namely regulation, which is most expensive [18].

However, several challenges are affecting the practical implementation of V2G technology. It has been announced that intermittent or even regular charging and discharging behavior can reduce battery life onboard the vehicle and incur faster replacement [19]. It is also mentioned by researchers about how challenging it is to meet the need of strong interaction between vehicles and the grid [20]. Even though the challenges have not been

overcome for now, researchers are optimistic about the future of V2G technology as intelligent control strategies are being developed and experimental results showed a reduction of 17% of peak demand compared to business-as-usual (BAU) scenarios if V2G charging is smartly used [5]. Also, although the lifespan of onboard battery in PEVs could be lowered for using V2G, it may still be considered more economical for both vehicle owners and grid companies to deploy V2G and possible battery changes accordingly [20].

2.4 Energy Storage Systems in the Power Grid

Serving as one of the most important parts of Distributed Generation (DG) systems, energy storage systems (ESS) enable decentralized intermittent grid power sources and modularize each part to enhance overall reliability and resilience. If power from the ESS system is properly managed, economic profits can be generated through market interactions with the utility grid network. The general idea behind the operation of an energy storage system is to store the power generated during the time when load demand is at a low level and electricity price is cheap accordingly, then release the stored power at peak load time when the price is high. Aside from traditional storage platforms such as batteries and pumped hydroelectric dams, the coupling of battery storage with PV power generation has also gained much popularity since the start of the 21th century.

Wind power is well-known for its uncertainty and fluctuations when it comes to power generation, making it hard to provide consistent energy to grids [21]. The coordination of ESS and wind power, reportedly, can suppress the instability of wind power output by having Q-learning in reinforcement learning to operate the system [22]. It is also pointed out that distributed and aggregated ESSs are similarly capable of effectively alleviating wind

power fluctuations too [21]. In an effort to control the ESSs when it comes to planning problems such as the optimal sizing of ESSs [23], mixed-integer programming (MIP) has been effectively used to design and dispatch the system and reduce ESS investment costs [24].

It is especially interesting when ESSs are integrated with a smart grid. One smart energy management system (SEMS) consisting both of energy storage parts and optimization parts has been developed for a microgrid and optimal operation strategies for economics have been discovered [25]. It has been further pointed out that with the right sizes and types of ESSs a net present value (NPV) can be maximized and acquired [26].

2.5 Transition from Macro Grid to Microgrid

The miniaturization of the power grids started about two decades ago when renewable distributed power sources were being introduced and when both manufacturing technology and far-reaching large-scale blackouts drove electric service providers into upgrading their already aging facilities. One solution proposed by the Consortium for Electric Reliability Technology Solutions (CERTS) after a 2003 blackout was to place generation closer to loads [27]. Routinely using renewable energy sources and energy storage systems (ESS) [28], microgrids can run separately from centralized macro grids autonomously. Increasing use of distributed energy resources (DER) in microgrids has led to the control conundrum of DER especially in terms of reducing carbon footprint [29]. One case designed deploying mixed integer linear program (MILP) discussed sizing and application of DER system in order to minimize cost as well as carbon emission [30].

Although microgrids have become popular lately, switching from the existing utility grid network model to microgrids can be difficult. One possible way is by using Virtual

Power Plant (VPP) technology. Not aiming at changing the way DG systems are connected to the grid, VPPs enhance the controllability of Distributed Energy Resource (DER) systems such as EVs and wind farms [31].With the help of VPP, commercial electricity markets are also believed to profit more by effective measures taken with more accurate anticipation of demand as well as higher decrease in charges caused by the gap between demand and generation. It is argued that one specific bidding strategy within the field of Commercial Virtual Power Plant (CVPP) enables the service provider to profit from more precise Day-ahead (DA) planning [32]. It has also been stated that based on direct load control (DLC) a VPP optimization algorithm was developed and helped reduce imbalance between power generation and consumption [31].

Some kinds of commercially available software or platforms are also capable of solving the upgrade problem. RNM-US, a coordinate-based platform using Reference Network Model, claims that given the GPS coordinate and power of each node it can build the microgrid either from scratch or based on existing energy sources [33]. It is also argued that algorithm based on MILP and transformer constraints achieves DER design and optimization in the microgrid by achieving Zero Net Energy (ZNE) [34].

2.6 Microgrid Topology Design

A successful microgrid system is always the key to quality microgrid design. With the promise of microgrid in mind, the popularity of microgrid design has been skyrocketing in recent years. Normally, existing microgrid design can be divided into three general categories: microgrid control design, microgrid topology design and hybrid of both.

Microgrid control design or planning focuses on optimization of microgrid operation.

Several control design strategies have been published. In 2015, a distributed cooperative control strategy for ESS in regards of local power balance related to charging/discharging efficiency was proposed [35]. A control strategy on various layers of hierarchical control architecture of microgrid on par with traditional power system also proved economically efficient in 2016 [36]. It is worth mentioning that a model predictive control approach based on MILP algorithm was presented to optimize time-variable goals such as optimum charge/discharge schedule [37].

Microgrid topology design, on the other hand, can be categorized into two kinds, one being planning and building from scratch to get desired conditions, the other being refurbishment and upgrade from existing topology. Some relevant studies are found and listed in accordance with the first criteria mentioned for microgrid topology design. Based on survivability schemes, one topology design involves a reconnection of a few small microgrid network communities which changes over time, aiming at reliability by optimized harness of renewable energy sources [6] . Topology design in [38] and [39] efficiently combines graph partitioning algorithm with MILP to reach local energy equilibrium when generating islands and remaking connections for mesh circuits. Multi-Objective Substrate Layer Coral Reefs Optimization Algorithm (Mo-SL-CRO) was applied by Jiménez-Fernández, S et al. to decide distribution of DERs and optimal connection of different nodes [7] .A viable restructuring of existing microgrid using phase angle measurements of the swing equations was announced by S. Talukdar et al. based on multivariate Wiener filtering to reconstruct operating radial power grids [8].

Fewer research for the other kind have been initiated compared to the first one. One interesting probabilistic reliability index based topology design has been proposed to partition the grid system into microgrids after optimizing reliability or a combination of reliability and

supply-security [40]. A novel robust optimization approach suggested by F. S. Gazijahani et al. enables researchers to determine allocation and parameters of key elements of microgrid such as DG and ESS before island existing grid into reconfigurable microgrids with profit and reliability considered [41]. Another option to optimally add and configure DG on existing grid circuits without changing original connections was proposed by M. V. Kirthiga et al. using sizing algorithm for an autonomous operation [42].

Normal aspects considered for microgrid design are assorted, usually depending on the design task the researchers are given. Reliability is probably the most considered factor. For instance, [6] and [39] all depict reliability as optimization goal, with one using renewable energy occupation maximization and the other using cooperation of loop design and performance index to reach the goal. Local power balance within islands is also popular. One topology design in [38] describes how efficient partitioning of grid can influence power supply/demand balance within each island generated. In [43] a supervision design to predict DC microgrid power flow with multiple factors considered using ILP algorithm was developed. Financial profit is another point commonly seen for consideration. [44] and [45] illustrate the increase of grid profit by risk-constrained stochastic programming and game theory, respectively. A novel block-chain involved microgrid design proposed by Tsao, Y et al. optimizes the use of renewable energy units to gain network profit along with reduced risk by robust type-2 fuzzy programming [46].

Some papers also take into consideration special requirements along with the normal aspects mentioned above. First to mention, some paper specially aims at a certain type of circuit type. For instance, as discussed in [47], Qin, M et al. applied extended DistFlow model of AC-OPF to the problem and an MILP algorithm involved method was proposed to solve operation of ESS specifically in radial networks; [48] investigates the coordinated

control of radial grid system with multi-agent system (MAS). On the contrary, [49] discussed the availability of using small mesh circuits in the grid as control route for PV monitoring, while another scenario including small scale mesh connections is discussed in [50] using modified L1 Adaptive control method. [38] and [39] are designed for mesh grids as well.

Also, grid type in terms of special types of electricity is another special feature that is sometime considered for research purpose. While most research exploit AC grids, such as [51] [52] [53] [54] [55], several papers have set their concentration on DC microgrid topology design. [56] presents a fuzzy control method for DC microgrid by design an energy management system (EMS). [57] proposes a control strategy involving two Synchronous Reference Frames for a DC microgrid. Some research even goes as far as AC/DC hybrid microgrids, such as that designed and evaluated in [58], [59] and [60].

3 Goal

The goal of this thesis is to develop and apply techniques for optimal design, dispatch, and reliable operation of alternative energy sources and storage systems in a disadvantaged community microgrid.

4 Objectives

To meet the thesis goal, five objectives are established as follows:

1. Conduct a thorough literature review on grid simulation and optimization applications and electrical vehicle roles in a smart grid as well as other related technologies.
2. Generate reliable EV charging load profiles and estimate charger counts based on information provided by NREL's Electric Vehicle Infrastructure – Projection (EVI-Pro) tool to use in the Oak View MicroGrid (OVMG) project.
3. Verify DERopt results for optimal sizing and dispatch of DER in the OVMG by comparing them to E3 RESOLVE model results.
4. Create a model for the OVMG system in the platform of OpenDSS.
5. Model the abilities of the OVMG to support the Southern California Edison grid and generalize microgrid capabilities for supporting high renewable penetration in the macro grid.

5 Approach

5.1 Task1 – Literature Review

In this task a thorough literature review on grid simulation and optimization applications and electrical vehicle roles in a smart grid as well as other related technologies is accomplished. The literature review is conducted to obtain the background knowledge of PV system, wind farm, energy storage system, electrical vehicle and roles they play in the power grid. Transitions from macro grids to microgrids will also be reviewed to gain knowledge about possible software, algorithm and technologies to achieve the upgrades. Some microgrid-based platforms such as DERopt will also be included in literature review.

5.2 Task2 – Electric Vehicle Simulation

In this task reliable EV charging load profiles of different types of microgrids and estimate charger counts based on information provided by NREL's EVI-PRO tool are generated to use in OVMG project. Different levels of EV charging demand are considered to generate reliable load profile. Based on information provided by NREL's EVI-PRO tool, one scientific way to estimate the EV charging demand will be determined which requires downscaling the EV charging load profile of Orange County to Oak View Community. After EV charging loads are determined, a model to approximate the charger count is developed and applied using all the information in the task.

5.3 Task3 – DERopt Verification

In this task DERopt results are verified by comparing them to E3 RESOLVE model results. The DERopt results are verified using the same or similar system, financial, technology and user parameters as E3 counterpart case. Modifications of parameters beyond those directly from E3 interface are required to simulate the Oak View Community situation. Power dynamic profiles including several DER technologies such as PV system by both DERopt and E3 are generated to compare and evaluate the results.

5.4 Task4 – OpenDSS Model of the OVMG

In this task a model for the Oak View microgrid system is created in the platform of OpenDSS. Based on SCE's DERiM Project, a topological model of Oak View Community is created using OpenDSS platform. Real-life based coordinate system of each generator, transformer and load will be determined to generate the map and potential field trips may be required. To determine the actual line and transformer parameters, data from American Wire Gauge (AWG) are harnessed to image the real impedance condition. For the load from different types of customers, which includes both residential and industrial load, URBANopt system as well as E3 platform are potentially used to reflect the real-time data profile.

5.5 Task5 – Evaluate Microgrid Performance

In this task the abilities of the Oak View microgrid to support the Southern California Edison grid and generalize microgrid capabilities for supporting high renewable penetration in the macro grid are simulated and evaluated. Based on the topological map built during

Task 4, a model is developed based on simulation experiments to determine the possible performance, potential position of smart switches that determine the interactions between the Oak View microgrid and the macro grid. Certain levels of DER and ESS are added to address the resiliency.

6 Model Development

6.1 Oak View Community Topology Construction in OpenDSS

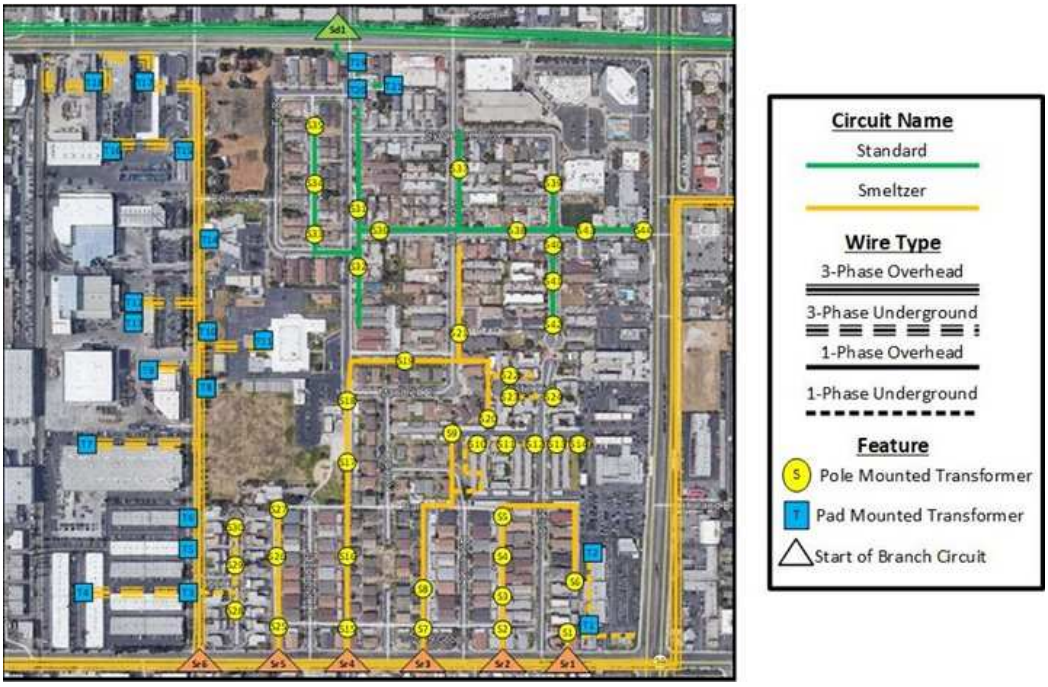

Figure 1 Oak View Community topology (not showing Beach 12 KV Distribution Circuits and Oceanview Substation)

The real-life example used in this thesis is the Oak View Community located in Huntington Beach, California. The electric distribution model was developed using the alternating current (AC) power flow simulator OpenDSS [61]. The OpenDSS tool can capture the complete resolution of three-phase voltage and current through distribution power lines and transformers. The western section of the community consists of commercial and industrial plants and offices along with Oak View School. The rest of the community are majority residential. Distribution system topology of Oak View Community in OpenDSS was

developed in three steps. The first step is to outline Oak View Community electric grid connection from SCE's DRPEP tool [34][62].

Secondly, on-site inspections were made to record and verify circuit connections, transformer types, ratings, locations and belongings, single phase existence and usage, and to revise them if necessary. Underground transformers and cables were believed to exist on the western commercial and industrial side of the community. In case of both underground and unmarked or unobservable transformers above ground, estimated ratings were given and will be discussed later. Wire rating and gauge were unobtainable as well, therefore discuss and assumptions will be made on them.

The last step is to combine the outlined the grid topology and information gained from field walks and a preliminary OpenDSS topology was made and then refined. This model was exercised using the tuned electrical demand results from the Oak View community energy simulation developed in URBANopt. In instances where wire ampacity limits were violated in the power flow simulation, wire diameter size was increased to avoid over-ampacity issues. In instances where transformer power limits were exceeded, building – transformer connections were first examined to ensure correct linkages. If overloads continued to occur after any changes to the model, transformer ratings were increased to the proper kVA rating. Wires were also sized using OpenDSS results. Complete transformer rating and revision have been attached in Appendix A.

Gauge selection occurred on an ampacity basis, ensuring that the baseline model would produce no over-ampacity conditions across all circuits. American Wire Gauge (AWG)[63] standards were used to select from. Wire conductor material is not known but is assumed to be copper. Sizing wires based on copper cable ampacity limits show that all residential circuits can receive utility service using 6-gauge wire. The commercial and

industrial circuit, however, requires 2-gauge wire at the start of the circuit, followed by 6-gauge wire sizes along the remainder of the length of the circuit. Only 6% in length of total commercial branched circuit is comprised of 2-gauge wire.

Existing topology of the Oak View Community is depicted in Figure 1. Branch SR1-SR5 and SD1 are all residential branches, whereas SR6 is the only commercial and industrial branch. Oceanview Substation (not present in Figure 1) is located in the Northeast corner Oak View Community and powers multiple local areas, including the Oak View Community. The Oak View Community is believed to consist of 1,1000 utility customers.

6.2 EV Charging Profile and Charger Count Estimation

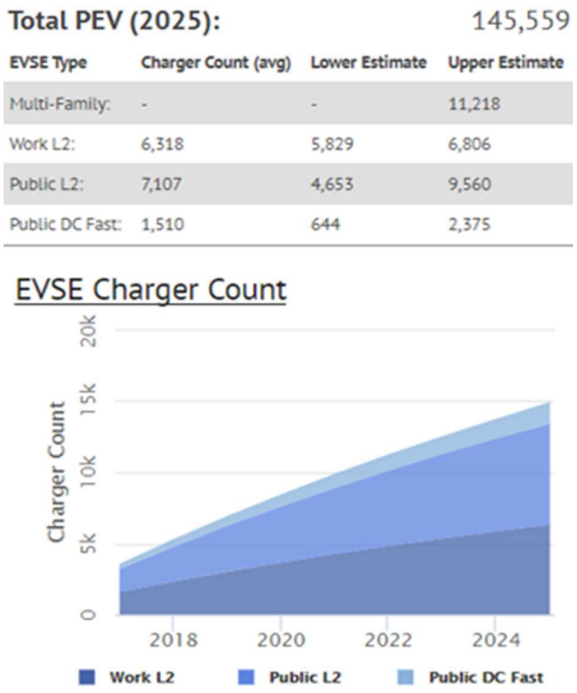

Total PEV (2025): 145,559

EVSE Type	Charger Count (avg)	Lower Estimate	Upper Estimate
Multi-Family:	-	-	11,218
Work L2:	6,318	5,829	6,806
Public L2:	7,107	4,653	9,560
Public DC Fast:	1,510	644	2,375

Figure 2 EVI-Pro: Orange County Total PEV and EVSE Charger Count in 2025 [64]

Table 1 - EVSE charging power levels assumed in EVI-Pro [65]

Charging Level (EVI-Pro)	**Home L1**	**Home L2**	**Work L2**	**Public L2**	**DC Fast**
Power capacity	1.4 kW	3.6-11.4 kW			50-105 kW

The goal of this section analysis is to generate different types of EV charging profiles and quantify the charging counts of different levels needed for a forecasted (2025) Plug-in Electric Vehicle (PEV) charging demand. Our test case is based upon the Oak View Community. Details about the Oak View Community have been discussed in section 6.1. Five different charging power levels are assumed to be used by Oak View infrastructure: Home L1, Home L2, Work L2, Public L2, and Public DC fast charging.

We use PEV infrastructure numbers, projected for 2025, calculated by the Electrical Vehicle Infrastructure Projection tool (EVI-Pro) developed by NREL [64]. The tool uses CHTS travel data, commercially available PEV technical specifications, and infrastructure attributes to estimate current and future PEV charging infrastructure to meet demand [65].

The EVI-Pro tool reports data such as *Total PEV, i.e.,* the projected count of PEVs in a particular geographic area, and the Electric Vehicle Supply Equipment (*EVSE) Charger Count* to supply the local PEV, as well as the time-resolved (10-minute) charging *Load Profile* for different charging power levels, for weekdays and weekends. Dataset for Orange County will be downscaled to represent Oak View, which will be described in 6.2.1. Figure 2 illustrates the dashboard view of the EVI-Pro tool dataset for Orange County.

6.2.1 OAK VIEW HOURLY PEV CHARGING DEMAND

To obtain the hourly charging demand in our Oak View community, as discussed earlier EVI-Pro data for Orange County will be scaled down accordingly. Assumption is

made that the hourly PEV charging demand for a given location is dependent upon its (1) PEV charging infrastructure, or EVSE count, and (2) PEV count (which in turn depends upon the local population and PEV adoption rate, *i.e.*, PEV per person). A downscaling factor has been defined, the *PEV ratio,* to be the ratio between the PEV count in Oak View and PEV count in Orange County. We use this ratio to calculate the PEV count in Oak View and EVSE infrastructure needed to supply this demand.

EVI-Pro forecasts that in 2025 there will be 145,559 PEV in Orange County ($n_{PEV,OC}$), but the projected 2025 PEV count in Oak View ($n_{PEV,OV}$) is unknown. The local population for these areas is known, so we obtain $n_{PEV,OV}$ by assuming that the PEV adoption in Oak View and Orange County is the same. The projected 2025 Orange County population is 3,349,664 people [66], while the 2017 Oak View population is about 9960 people [67], and using a 0.15% annual growth ratio (the OC population growth rate), the projected 2025 Oak View population is 10,080 people, as described by Equation 1. In, Equation 2, Oak View's PEV count is calculated to be 438, and therefore, the *PEV Ratio* is 0.0030, as shown by Equation 3.

$$n_{population,OV} = 9960\ (1 + 0.0015)^8 = 10{,}080\ people \quad (1)$$

$$n_{PEV,OV} = n_{population,OV}\left(\frac{n_{PEV,OC}}{n_{population,OC}}\right) = 438\ PEV \quad (2)$$

$$PEV\ Ratio = \frac{n_{PEV,OV}}{n_{PEV,OC}} = 0.00301 \quad (3)$$

We use the *PEV Ratio* to calculate the Oak View EVSE count.

Table 2- EVSE count for Orange County and Oak View, broken down by charging level [64]

EVSE Charging Power Level	**EVSE count for Orange County**	**EVSE count for Oak View [2]**

Home L1	131,003[1]	394
Home L2		
Work L2	6,318	19
Public L2	7,107	21
Public DC Fast	1,510	5
Total	**145,938**	**439**

(1) Assumed that 90% of the PEV count charges on residential (Home L1 + Home L2) [65]

(2) Orange County data from EVI-Pro scaled down by the PEV Ratio

6.2.2 EVSE CLUSTERING

Oak View hourly PEV charging profiles need to be broken down into representative clusters of EVSE before they can be judiciously allocated into the Oak View building nodes and connected to the existing electric infrastructure. This section will discuss EVSE clustering.

Total EVSE count were first divided for each charging power level by the number of transformers that will host the infrastructure for the appropriate customer class (Residential, Commercial, or Industrial). For instance, nine residential transformers will host Home L1 charging and one residential transformer that will host Home L2 charging, with a total of 10 transformers. The Oak view EVSE count for Home L1 + Home L2 is 394 (minimum infrastructure needed). Therefore, we allocate 10 clusters of 40 for a total of 400 chargers. Same logic was applied to the other categories, and the results are shown in the "Clusters" column of Table 3.

Table 3 - EVSE clustering: Transformers available for each charging power, total EVSE count per cluster and total clusters to be allocated in Oak View

Charging Power Level	Transformer Count	EVSE count	Clusters
Home L1	9	394	10 clusters of 40
Home L2	1		
Work L2	5	19	5 clusters 4
Public L2	3	21	3 clusters of 7
Public DC Fast	1	5	1 cluster of 5

The final Oak View hourly PEV charging profiles for each EVSE cluster are then obtained by normalizing the Orange County hourly PEV charging demand (by the appropriate EVSE count, from Table 2, *EVSE count for Oak View* column) and then multiplying by the appropriate PEV cluster size from Table 3, *Clusters* column). This scaling/clustering logic was used for all charging power levels except for DC fast charging, where we noted that the normalized demand did not represent a realistic charging profile since the hourly peak charging power was significantly lower than one single EVSE rated power (~50kW), by one order of magnitude.

Thus, instead of normalizing the Orange County data by the EVSE count provided EVI-Pro (1510), we calculate the number of peak charging sessions from the raw data by dividing the peak charging demand, in kW, by our assumed average DC fast charging power level (50 kW) as shown in Equation (4). Our primary underlying assumption is that one charging session corresponds to one EVSE. We then assume that the EVSE infrastructure used at peak belongs to a percentile of the total EVSE infrastructure. Therefore, the total *EVSE Count* is calculated by dividing the Peak Charging Sessions by the appropriate percentile, as shown in Equation (5). Assuming all DC Fast charging EVSE used at peak charging correspond to the 90^{th} percentile of total infrastructure, we obtain a total DC Fast

EVSE count of 157. We use this value to normalize the Orange County data and scale it up to produce our 5 EVSE cluster.

$$Peak\ Charging\ Sessions\ =\ \frac{Peak\ Charigng\ Demand}{EVSE\ Power} \tag{4}$$

$$EVSE\ Count\ =\ \frac{Peak\ Charging\ Sessions}{Percentile} \tag{5}$$

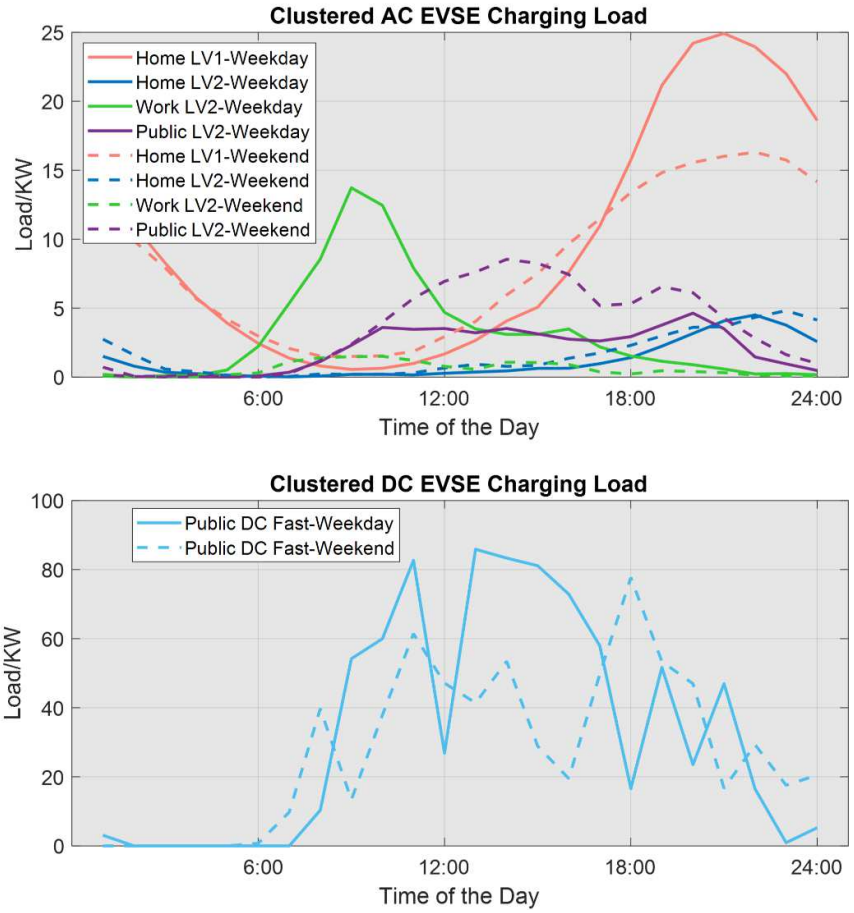

Figure 3 - Hourly PEV Charging Profile for EVSE clusters: Home L1, Home L2, Work L2, Public, L2, and DC Fast charging. Solid lines represent charging demand on weekdays. Dashed lines represent charging demand on weekends.

Figure 3 shows the resulting clustered Oak View hourly charging profiles for the five different charging levels assumed: Home L1, Home L2, Work L2, Public L2, and DC Fast Charging, separated by weekends and weekdays.

On weekdays, the Home L1 cluster of 39 PEV peaks in the evening at 27 kW at 9 PM. Weekend demand is overall lower. The data distribution shows a standard deviation of 9 kW. The Home L2 cluster of 39 PEV peaks at 31 kW at 10 PM on weekdays, and similarly to Home L1, it also shows a slightly lower demand on the weekends. The data distribution also shows a standard deviation of 9 kW. Work Level 2 cluster of 4 EVSE peaks at 15 kW at 9 AM, with significantly lower demand on the weekends. The data distribution also shows a smaller standard deviation of 4 kW. The cluster of 5 Public L2 EVSE, on the other hand, peak at 10 kW on the weekend, at 2 PM – weekend demand is higher than weekday demand. The data distribution also shows an even standard deviation of 3 kW. Finally, the cluster of 5 DC fast chargers peaks at 85 kW on weekdays at 1 PM and 80 kW at 6 PM on weekends with a standard deviation of 40 kW.

6.3 Verification of DERopt profiles in E3 RESOLVE Tool

E3 RESOLVE [68] is an industry-grade Excel-based energy solution provider that combines ACPF analysis, energy market optimization and investment friendly UIs. DERopt generated baseline power profiles were used as input in E3 RESOLVE tool to confirm its practicality and accuracy. Profiles used as inputs were listed in Table 4.

Table 4 E3 RESOLVE input from DERopt

Input	**Categories**
Weather Data	Dew-point Temperature
	Dry-bulb Temperature
	Windspeed
Load Shapes	Electric Demand
Storage	ESS charge/discharge Profiles
PV Rating	PV Sizes

PV	PV Profiles

Figure 4 presents the dashboard view of E3 RESOLVE dataset for Oak View Community.

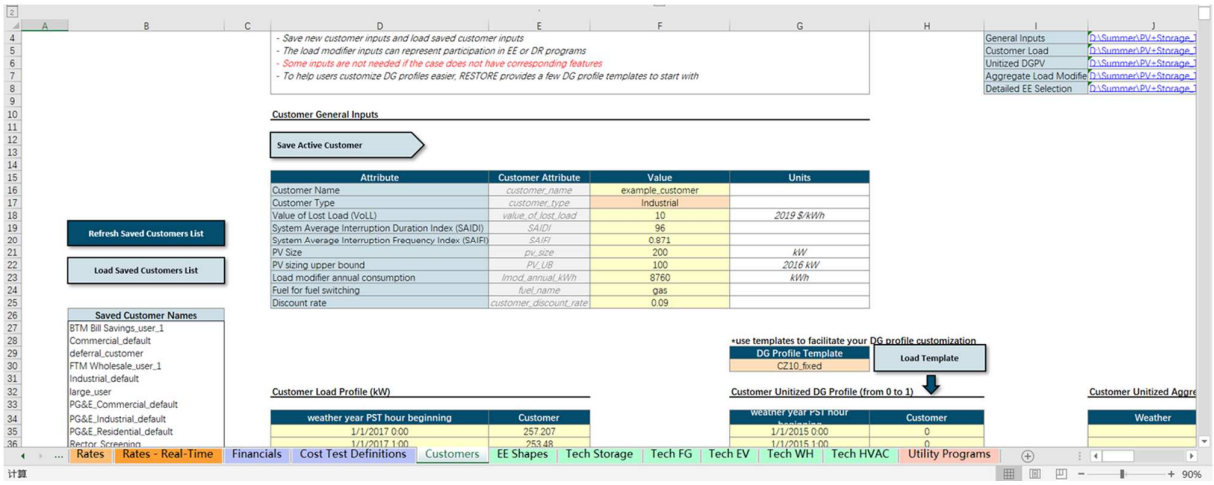

Figure 4 E3 RESOLVE User Interface using Oak View Community settings

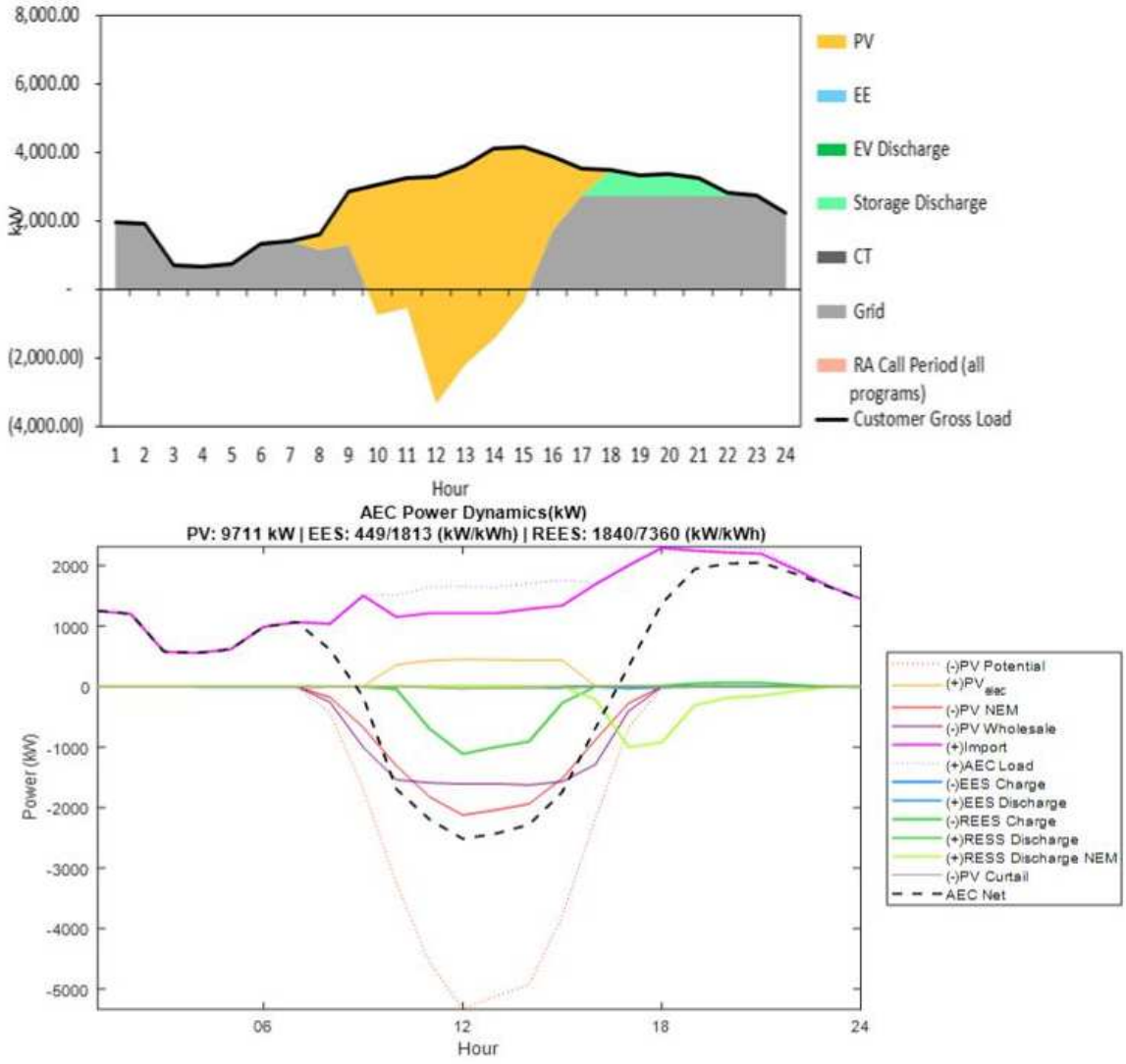

Figure 5 E3 RESOLVE and DERopt showcase ACPF breakdown on January 3rd

Table 5 DERopt outputs that are not captured by E3 RESOLVE model

Output of DERopt	Description
PV Potential	Full PV Potential
PV_{elec}	fraction of the load that is met by all PV systems combined
PV Wholesale	PV power exported under wholesale rate
ESS Charge	Charging dynamics of Electric Energy Storage (ESS)

RESS Charge/Discharge	Charging/discharging dynamics of Renewable Electric Energy Storage (RESS)
RESS Discharge NEM	RESS discharging dynamic under net energy metering (NEM)
Import	fraction of the load met by external imports (at the building level)
PV Curtail	Net-Energy flow through the AEC

A showcase of power breakdown results for both E3 RESOLVE tool and DERopt on January 3rd was selected and is depicted in Figure 5. AC power import using both tools was confirmed to be on very similar level. Same parameters from Table 4 were used for both models to generate the power dynamics of our OVMG baseline ACPF. As is shown in Figure 5, PV energy output and storage discharge output are on similar level for both models, which is represented by marker PV/PV NEM and Storage Discharge/RESS Discharge NEM, respectively. It can be concluded that both DERopt and E3 RESOLVE consider PV and ESS/RESS net energy metering (NEM) rates.

Although both share similar results of same types, DERopt is also able to capture more information. Additional profiles that are only captured in DERopt are documented in Table 5. While DERopt is able to capture more detailed operational information of PV and ESS/RESS, E3 RESOLVE model stands out by the ability to harness more technologies, including various types of fuel cell, which is represented CT in Figure 5.

6.4 Microgrid Topology Design

Oak View Community is made up of radially distributed branch circuits. As discussed earlier in Literature Review, very few methods were developed for and consider real-life

based radially developed grid/microgrid system. To fill in the gap, in this section, a real-life based Oak View Community microgrid system which is composed of radial circuits is developed, and a topology optimization methodology is applied to the microgrid while keeping the majority of the original connections to be practically achievable. Inspired by [38], a revised Multilevel Graph Partitioning algorithm combined with Mixed-integer linear programming (MILP) is applied to the microgrid. The results present the initial realization of resilience and efficiency within community.

The topology design process consists of two stages, Stage 1 and 2. Stage 1 is the graph-partitioning-based loop planning, where different recommended islands are generated and positions of switches to switch to island operation mode can be determined during emergency situations. This Stage comprises Three Phases; Phase-1 coarsening, Phase-2 Partitioning and Phase-3 Uncoarsening and Refinement. Stage 1 contributes to generation/load balancing and potential to manage islanded operation. Stage 2 is the ILP-based Loop Structure Design process, where the MILP algorithm was harnessed to determine how extra connections can be made within each island. Stage 1 is realized in MATLAB with OpenDSS output results, while Stage 2 is achieved with help from MATLAB and results after each of the stages will be shown.

Graph Partitioning Algorithm

Original multilevel graph partitioning algorithm are described as follows. The application and adaption of the algorithm to tailor our specific needs for radial microgrid will be discussed.

Given a graph G=(V,E) with weights on all vertices and desired partitioning part number N, one way to partition G into N different parts with goals of keeping the sums of vertex in each part as equally close as possible and weights of edge crossing those N parts

minimized is multilevel graph partitioning method. The 3-phase algorithm can be described as follows.

The Coarsening Phase

The original graph G is reduced into a series of successively coarser graphs G_1, G_2,…G_N in this phase. Numerous ways to achieve this phase have been discovered, including Heavy Edge Matching (HEM), Light Edge Matching (LEM), Key Vertex Algorithm and Heavy Clique Matching (HCM). The first two are among the most popular, aiming at collapsing weighted edges of heaviest and lightest unmatched edge, respectively.

The Partitioning Phase

After contracting edges and making graph G into sufficiently small parts in Phase-1, partitioning can be easily done with many kinds of modern partitioners to partition coarsened graphs into small parts. Kernighan-Lin (KL) and Graph Growing Algorithm (GGP) are considered two of the most well-used partitioners. The overall goal of the phase is to equalize the total vertex weight of each desired N parts.

The Uncoarsening and Refinement Phase

In the final phase of the multilevel graph partitioning algorithm, each partitioned graph G_{i+1} is first projected back and inherited by graph G_i, which is called uncoarsening. Since no new edge matching is made, sum of vertex weight is perfectly preserved in each set of nodes. Local refinement procedures are implemented simultaneously with uncoarsening. Notably, popular Kernighan and Lin (KL) refinement gives each adjacent node set chances to further balance summation of vertex weight by relocating possible boundary vertices.

6.4.1 STAGE 1: GRAPH-PARTITIONING-BASED LOOP PLANNING

6.4.1.1 PHASE-1: COARSENING

Phase 1 is coarsening, where the graph is simplified into several node sets that are regarded as single nodes for partitioning in phase 2. The heavy edge matching (HEM) is used here, which is a highly efficient coarsening algorithm. The basic idea of HEM is to have neighbor nodes to join the given node to form a single node that has the relatively high-weight edges. Commonly seen in communication network problem, HEM in our case is slightly modified and the edge weight-based criterion is replaced by line length-based criterion, with the edge with shortest distance from the chosen vertex Vm being of the highest weight. A lower probability of being identified as an interconnecting line in the partitioning phase is assumed to exist for nodes with a short mutual distance, which guarantees closeness. The following modified HEM steps are followed:

a) Initialize the set of matching as $M_0 = \varnothing$; i=0;

b) Randomly select a vertex (V_m) in G_i that is not yet associated with the matching M_i;

c) Among edges adjacent to V_m, select the minimal length edge (maximal-weight edge) (E_{mn});

d) Join vertices V_m and V_n to form a new vertex in $G_i + 1$; associate V_m and V_n with matching M_i;

e) If the termination condition is satisfied (i.e., half of the total nodes are includes in coarsened graph, which is the criteria we chose) then stop; otherwise, set i=i+1 and go back to Step b.

a b c d

Figure 6 Phase-1 showcase in Oak View Community Industrial branched circuit

To help understand how Phase-1 works, an example of how our topology is developed in this stage and depicted in Figure 6. The branched circuit of Smeltzer 12KV distribution line located in the West part of Oak View Community is chosen for demonstration.

The branched circuit is shown in Picture a of Figure 6, where three-phase transformers are marked in yellow and connection lines are in orange. Both loaded and unloaded nodes are marked with numbers, as required by OpenDSS. The blue line at the bottom is Smeltzer 12KV distribution line, which powers the branched circuit; while the green line on top is Standard 12KV distribution line, with no connection to the part of branched circuit demonstrated here.

Picture b in Figure 6 described the first iteration of Phase-1. Each node randomly chosen for the iteration is circled in black, and is grouped with node with shortest distance, which process is represented by red lines. It is worth mentioning that in case two or more neighbor nodes share same shortest distance from a chosen vertex, one of them will be randomly chosen to be grouped. Once two or more nodes are in the same group, they share

same connection and distance to all their neighbor nodes. For instance, in b of Figure 6 node 65 and 66 after first iteration are both connected to node 67 and 68, the distance between the two groups being the same as distance between node 66 and 67 in a of Figure 6. Picture c and d of Figure 6 describes the last two iteration in Phase-1. Final iteration result shows the graph is small enough for partitioning in Phase-2, with a few groups containing more than two nodes.

6.4.1.2 PHASE-2: PARTITIONING

Phase-2 is partitioning. After each graph is efficiently small after Phase-1, less complex techniques were used for partitioning, including the widely applied greedy graph growing partitioning (GGGP) algorithms, which starts from initial vertexes then grows the vertex to cover a larger region towards a local optimum. The partitioning phase aims at further addressing of potential islanding and reaching local generation/load balance.

Unlike traditional partitioning phase in graph theory where randomly nodes are chosen to start with in Phase-2, modifications were made on the first step to start from top ranked DER nodes to ensure that when growing the loop system islands will maintain certain degree of power/load balance, which contributes to islands' self-healing ability, on top of potential to island operation. Similar to Phase-1, Phase-2 partitioning process is again weight-based. To better tailor the partitioning process to our specific need, modified weight/gain in consideration of both island operation potential and local power balance was used, as described in step (b). The following steps are followed:

a) Each loop (V1) starts to grow from one of controllable top X-ranked DER nodes

b) Vertex (V_m) in V1's boundary (V2) that has maximal Gain (e.g., reduction of edge weight in the cut-set of V_1) is inserted to V_1;

Gain definition: Gain(Vj) = $\frac{1-|mis(Vm)|}{dis\{Vj,Vk\}}$, where mis($V_m$) = $\frac{GC(Vm)-D(Vm)}{D(Vm)} \times 100\%$, dis{$V_j$,$V_k$} is the distance between node V_j and its closest first-order neighbor node V_k in V_m; and mis(V_m) is the power mismatch in loop V_m when node V_j is inserted ; DG capacity (GC) and average load (D).

c) The first-order neighbors of V_m previously belong to V_3 are moved to V_2;

d) If a given condition is satisfied (e.g., all nodes are included in different regions(V1,V2,…), which is the criteria we adopted), then stop; otherwise, go back to Step-b.

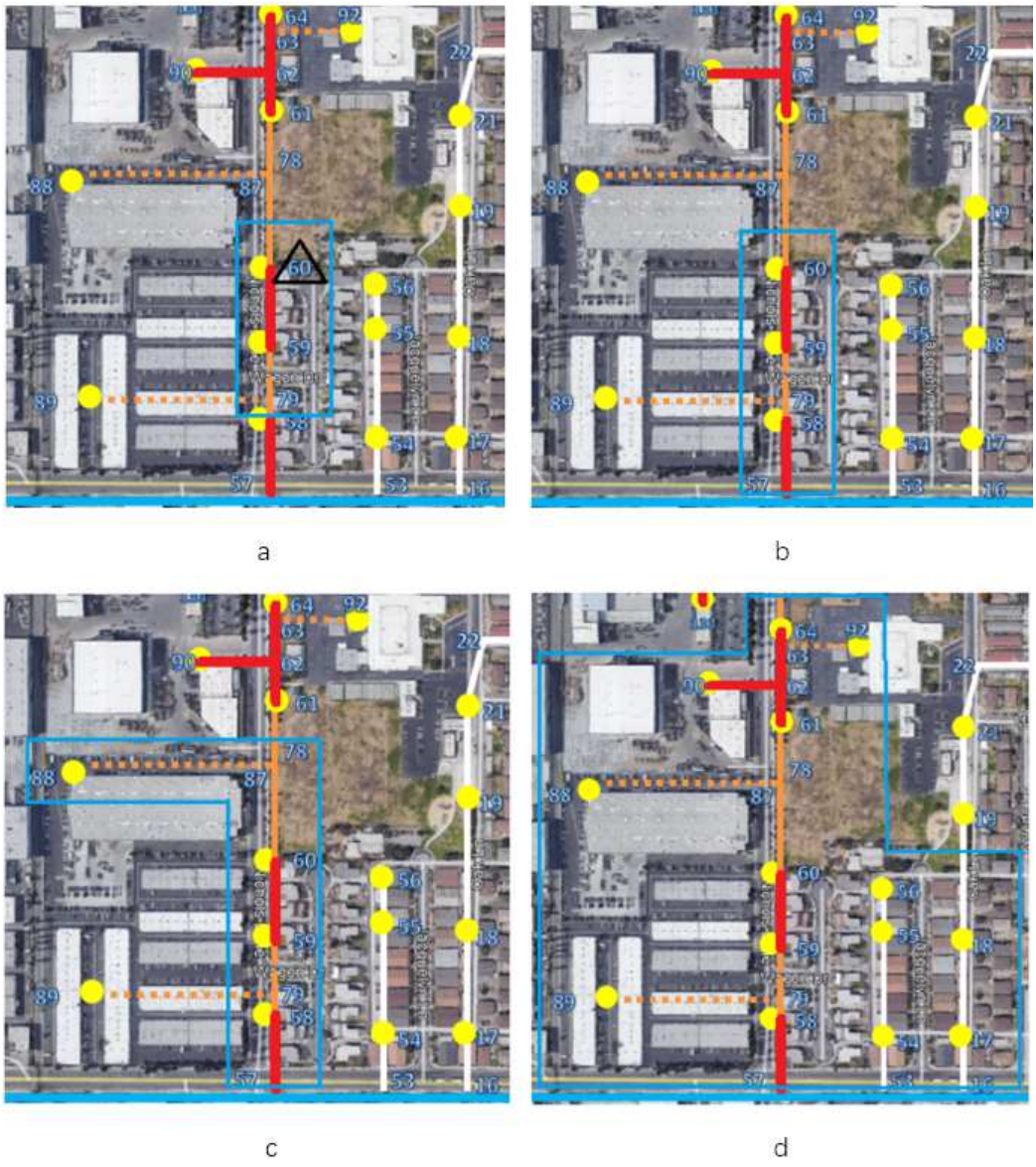

Figure 7 Phase-2 showcase in Oak View Community Industrial branched circuit

To help understand how Phase-2 works, an example of how our topology is developed in this phase is depicted in Figure 7. Showcase result contains 7 top-ranked DERs, and one specific DER nodes located in the Southwest corner of the Oak View Community—Node 60, will be examined.

From the chosen DER node/node set, the island grows with inclusion of one of its neighbor nodes or node sets in each iteration. Phase-2 stops when all nodes are incorporated

in different islands oriented from predefined DER nodes. Chosen DER Node, Node 60 is circled in black in picture a of Figure 7.

Picture a of Figure 7 illustrates how first iteration of Phase-2 works. Starting with Node 60 together with Node 59 as a group after Phase-1, the first iteration expands to include Node 79 from its neighbor node set— {Node 87, Node 79}, for Node 79 result in a bigger gain in our case when incorporated. The growing process is highlighted in blue. Picture b of Figure 7 demonstrates how our DER-oriented island grows in the second iteration. Neighbor node set considered this time are as follows: {Node 87, Node 89, Node group (57,58)}. The biggest gain is realized when node group Node 57 and 58 are included. Picture c of Figure 7 shows what the island is like in the fourth iteration. It is interesting that the growing process is not confined to nodes from same branched circuit. Picture d of Figure 7 shows the result of final iteration, the fourteenth iteration, and nodes from different radial legs/branches are included. After the last iteration, all 145 nodes are included in 7 islands growing from 7 predetermined DER nodes.

6.4.1.3 PHASE-3: UNCOARSENING AND REFINEMENT

Phase-3 of stage-1 is Uncoarsening and Refinement. Uncoarsening stands for the rewinding process of Phase-1. More specifically nodes groups are cancelled, and their internal and external connections are rescinded iteratively, and the computed partitions are projected back to the original graph by going through each step. Refinement, on the other hand, focuses on further narrowing down the gap between local power generation and demand by doing swap testing and performing successful swaps. Uncoarsening and Refinement procedure are done simultaneously.

Similar to two phases mentioned above, Phase-3 in our case is also modified. Our

criteria for doing swap testing, apart from keeping down generation/load unbalance, also focus on inviting nodes from branched circuit that are from different distribution 12KV circuit. The following steps are followed:

a) (Swap testing): randomly select a pair of boundary nodes and test if their swap can improve the current partition (e.g., successful or failed swap);

Revised the swap testing (step a) criterion:

$\lambda_{m,n}=\sum_{m,n}\{|mis(Vi)-mis(Vi)^{**}|+|es(Vi)-es(Vi)^{**}|\}\times$Distline_weight

Distline_weight= 1 if i is from different distribution line of m or n,2 otherwise.

es(Vi)= $\frac{EC(Vi)}{D(Vi)}\times 100\%$, i=m,n;

mis(V_i)** =$\frac{GC(MG)-D(MG)}{D(MG)}$;

es(V_i)** =$\frac{EC(MG)}{D(MG)}$

Where double superscript ** denotes the respective desired value, which can be defined with MG value denoting the entire microgrid. GC stands for DG capacity and D stands for average load, m and n denotes two adjacent loop systems.

b) Perform and only perform the successful swap (if λ is reduced then it is considered a successful swap).

c) Once a vertex is tested, it will be fixed (excluded from any future swap testing);

d) If a given condition is satisfied (e.g., there are n successive cancelled swaps where n is a predefined number), then stop; otherwise, go back to Step-a.

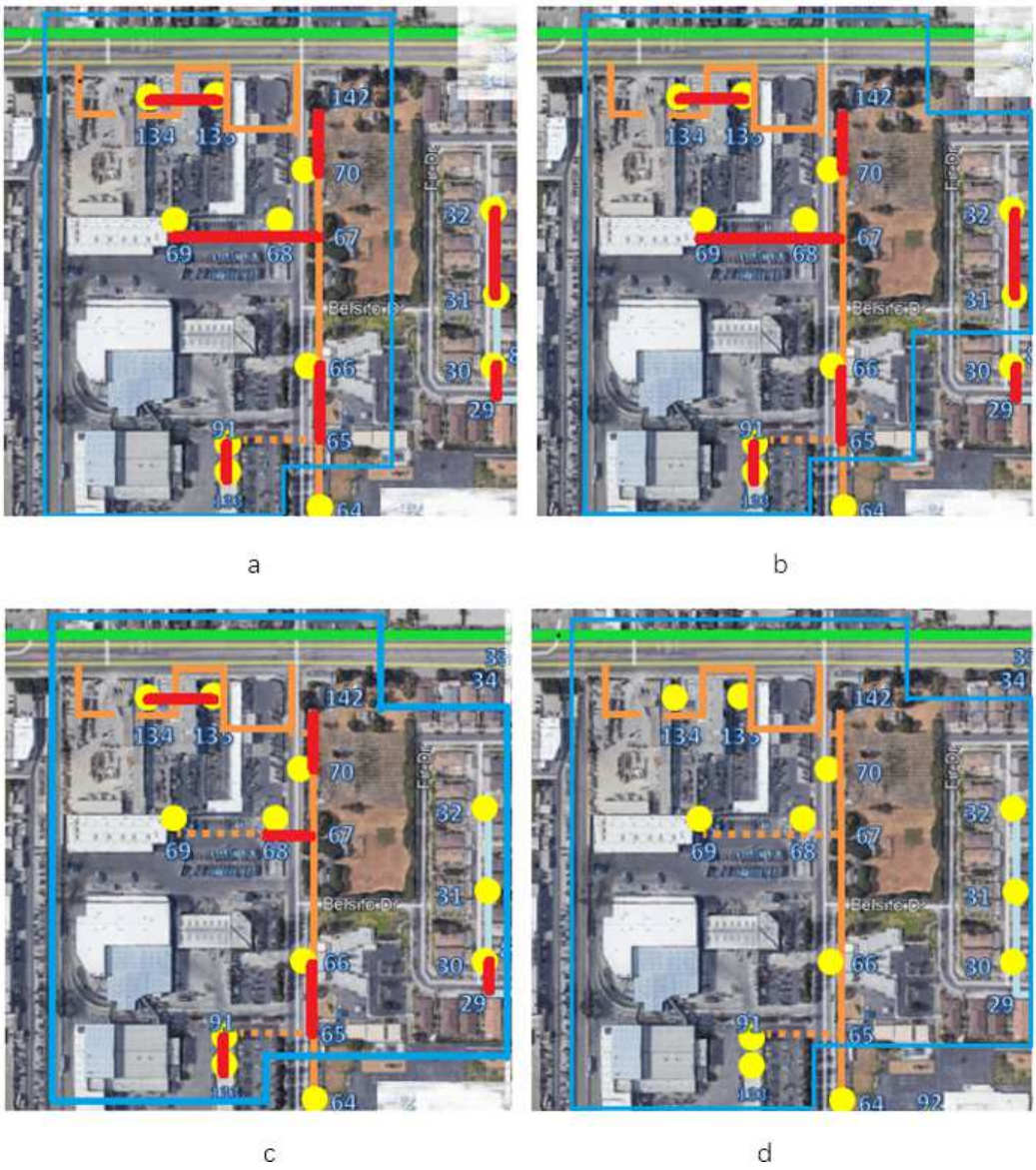

Figure 8 Phase-3 showcase in Oak View Community Industrial branched circuit

To help understand how Phase-3 works, an example of how our topology is developed in this phase is depicted in Figure 8. The showcase island is the upper part of what is illustrated as examples in Phase-1, where the green line is Standard 12KV distribution line that is not connected to the island. Red lines rescinding progressively in each iteration are kept showing how Uncoarsening process works, while update of nodes in the island aims at demonstration of the Refinement process.

Picture a of Figure 8 shows the final result of Phase-2, an island oriented with DER Node 70. Red lines imply grouped node sets. Nodes in blue circle are included in current islands, while other nodes shown in the picture (i.e., Node 29, Node 30, Node 31, Node 32, and Node 64 in picture a of Figure 8 belongs to other islands. Contrary to original swap testing where only boundary nodes that are physically connected should be considered (e.g., Node 64 and Node 65 in picture a of Figure 8, boundary nodes that share spatial closeness are considered (e.g. Node 32 and Node 67 in picture a of Figure 8. Since there are four iterations in Phase-1, three iterations in Phase-3 are necessary to project the graph back to original connections.

Picture b of Figure 8 described the result after first iteration. According to results in MATLAB, Node 67 (with Node 68 and 69 in the same note set) and Node 32 (with Node 31 in the same node set) are randomly chosen for swap test. By incorporation of Node 32 and Node 31 into showcase island and exclusion of the two nodes from the spatially adjacent island not shown in the figures, smaller λ is acquired and swap is implemented. This is a typical example of Refinement process. Interestingly, Uncoarsening process is also achieved in first iteration, though not present in picture b of Figure 8. Picture c of Figure 8 exhibits the result of the second iteration. Node 66 and 30 along with their node sets are chosen and successful swap test is performed. Uncoarsening process is also embodied, with Node 68,69 and Node 31,32 being ungrouped respectively. Picture d of Figure 8 features the third and final iteration of Phase-3, with no refinement and several uncoarsening happening to the island.

6.4.1.4 FINAL RESULT OF STAGE 1

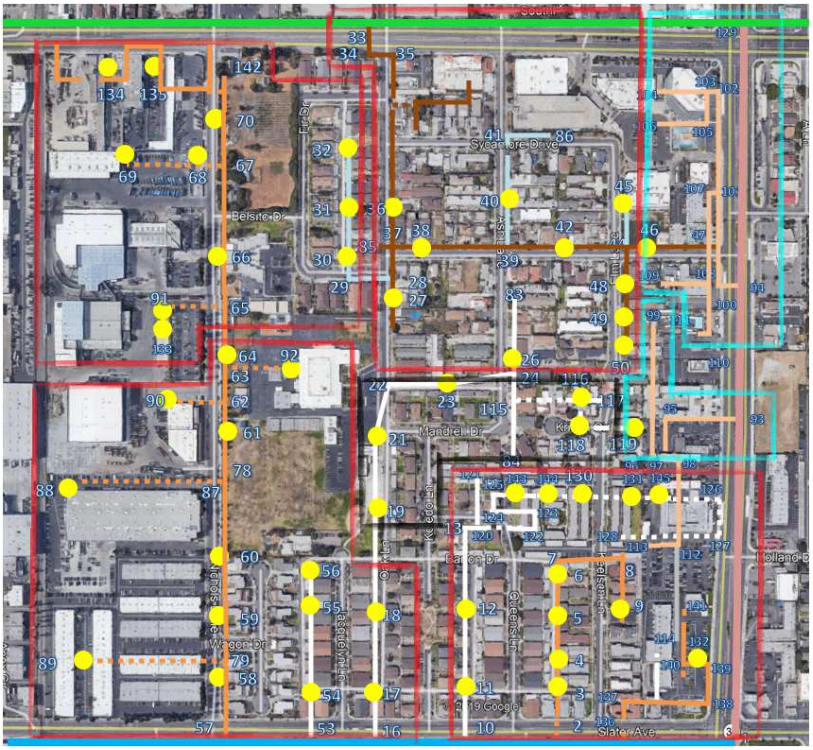

Figure 9 Final Result in Stage 1 for Oak View Community

Figure 9 shows the result after Stage 1. Different islands are circled in different colors (7 in total for now, can be changed). With existing connection maintained, several unlinked nodes will be connected in Stage 2. Potential position for switches can be determined in Figure 9 as junctions of each island. During normal mode switches are closed, while in emergency where island operation is the only option, these switches stay open and DERs and ESS will power different islands. The following section will discuss how extra connections for those missing links are made in Stage 2.

6.4.2 STAGE 2: MILP-BASED LOOP STRUCTURE DESIGN

In Stage 2, Mixed-integer linear programming (MILP) algorithm is harnessed. Based on famous Travelling Salesman Problem (TSP), our algorithm for each of islands in Stage 2 is applied is as follows:

$$Min: \sum \boldsymbol{i} \sum \boldsymbol{j} \boldsymbol{b_{ij} c_{ij} a_{ij}}$$

Subject to constraints:

$$1 \leq \sum_{j} a_{ij} \leq k \qquad \forall i = 2, \ldots, N\text{-}1 \tag{1}$$

$$\sum_{i} a_{Nj} = 0 \tag{2}$$

$$1 \leq \sum_{i} b_{ij} \leq k \qquad \forall j = 2, \ldots, N\text{-}1 \tag{3}$$

$$\sum_{i} a_{i1} = 0 \tag{4}$$

$$t_i - t_j \leq N \times (1 - a_{ij}) - 1 \qquad \forall i, j = 1,2, \ldots, N \tag{5}$$

$$a_{ij} \in \{0,1\} \tag{6}$$

$$t_i \in \{1,2, \ldots, N\} \tag{7}$$

$$L \leq \sum a_{ij} \leq k \qquad \forall i, j \; that \; b_{ij} < 1/2 \; \& \text{ are deemed high-risk} \tag{8}$$

$$b_{ij} = 1 - (Im_i + Im_j)/2 \tag{9}$$

$$a_{ij} = 1 \qquad \forall i, j \; that \text{ is connected in current existing topology} \tag{10}$$

For optimization constraints (1)-(10), i and j represents the parent and son nodes of line i-j. The decision variable a_{ij} is equal to 1 when line i-j is selected and is equal to 0 otherwise. Importance factor Im stands for significance of line i-j and is calculated by normalized load value of nodes (for non-load nodes Im is 0) in each island. The existence of Im and b_{ij} guarantees that an importance-based criterion is considered and power supply for critical load such as residential load is favored in case of emergency and islanded operation.

The value of the importance factor Im is shown in . c_{ij} represents for the distance of Node i and j. In our Oak View topology, c_{ij} stand for different cable segment and i, j represents different active nodes. (1) indicates that node i can have up to K son nodes while (2) ensures that the end node does not have any son node. (3)-(4) provide similar functions from the viewpoint of parent node. (5) eliminates any sub-loop within the loop system by introducing an integer variable t_i and is optional in our case. (8) & (9) ensures that node with higher importance is more likely to be able to get more energy route, while (10) ensures that existing connections are not disturbed. The reason for keeping original connections will be expanded on later.

Table 6 Importance factor value for different load types

Load Type	Importance Factor Im Value
Residential	1
Commercial	0.8
Industrial	0.8

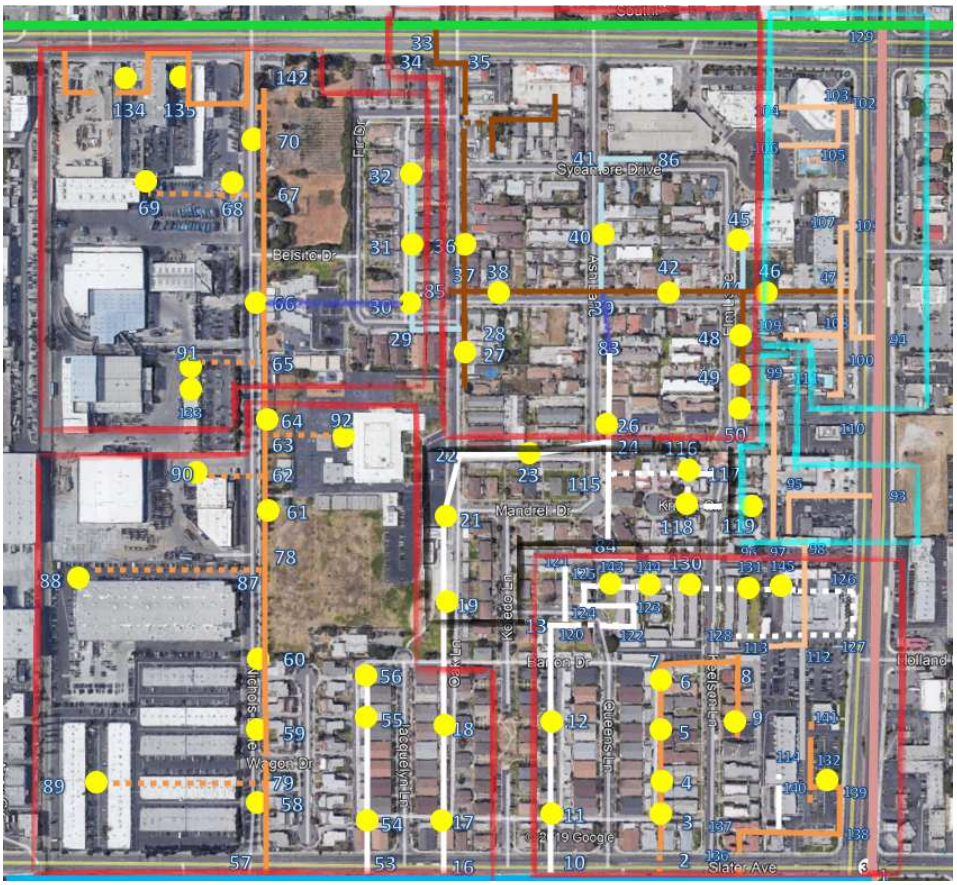

Figure 10 Stage-2 result with all constraints in Oak View Community

Figure 10 shows the result of Stage 2 when constraints (1)-(10) are all implemented. Several connections are made, and no mesh circuit is generated.

While the first stage combines enhancing local power balance, developing islanding possibilities and encouraging incorporation of radial circuits from different distribution lines, the second stage can be implemented based on importance-based upgrade while keeping most existing connections. The showcase example in Oak View Community has been divided into seven different islands. There was the intention to rebuild the community grid connections without the existing network, however, the practical engineering difficulty has made that sometimes unachievable. Therefore, Stage 2 also explores the possibilities with the existence of current network.

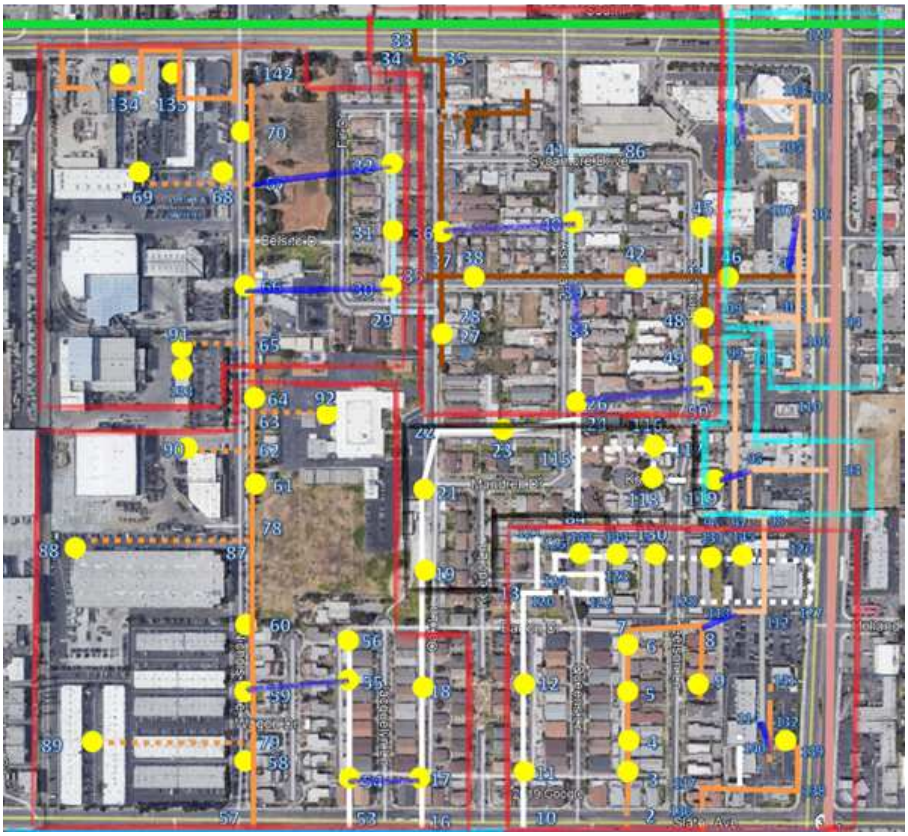

Figure 11 Stage-2 result without constraint (5) in Oak View Community

In comparison, when constraint (5) is not enforced, mesh circuits are available, accomplished by new connections either between nodes from different distribution lines or nodes from different radial legs from same distribution line in some islands, as shown in Figure 11.

6.4.3 RATIONALE FOR KEEPING EXISTING CONNECTIONS

a b

Figure 12 Comparison of results with and without using existing connections in the community

Picture a and b of Figure 12 details loop design with or without existing connections. Two figures shown are the same island before making connections (the upper left island with DER Node 70 as center in Figure 10). While it is possible that connections in the Picture b of Figure 12 may yield better results regarding power balance within islands and resiliency, it is obvious that some unrealistic links are made (e.g., link between Node 91 and 69), and geographical situation may not allow the direct connections of some nodes. For practical purposes, "ideal" connections without keeping existing connections is not considered in this Stage 2.

6.5 Test Scenarios

Nine different examples are used to demonstrate how the impact of DER and ESS in a real-life disadvantaged community was applied and evaluated and to show the effectiveness of the optimal topology design algorithm mentioned above. All scenarios are based on the

Oak View Community and its AC Power Flow model illustrated in 6.1. The nine scenarios can be classified into three categories based on EV penetration rate: Baseline scenarios with no EV adopted, Medium Penetration EV scenarios which are California 2025 State Goal compliant [65], as well as High Penetration EV scenarios that assumes 100% conversion of conventional vehicles to electric vehicles across the community. Each category consists of three different scenarios where the DER/ESS was or was not installed and both grid connected and islanded operation modes were explored. Baseline building electricity load profiles and DER profiles were developed using community scale energy simulation tool URBANopt [69]. DER installment almost covers every active transformer shown in Figure 1 and is on the same level of electric demand with EV charging demands of the Medium Penetration EV scenarios to be discussed below. Base KV is selected to be a Line-Line voltage of 12.5 KV, or 7.2 KV in Line-Neutral voltage. A summary of all analyzed scenarios is shown in Table 7.

Table 7 Test scenarios summary

OVMG Scenario (Both grid-connected and islanded operation mode if possible)		EV Penetration		
		Baseline (Zero EV Adoption)	2025 CA State Goal Compliant	100% EV Conversion
DER Penetration	0%	√	√	√
	Fixed Rate	√	√	√

6.5.1 BASELINE SCENARIOS

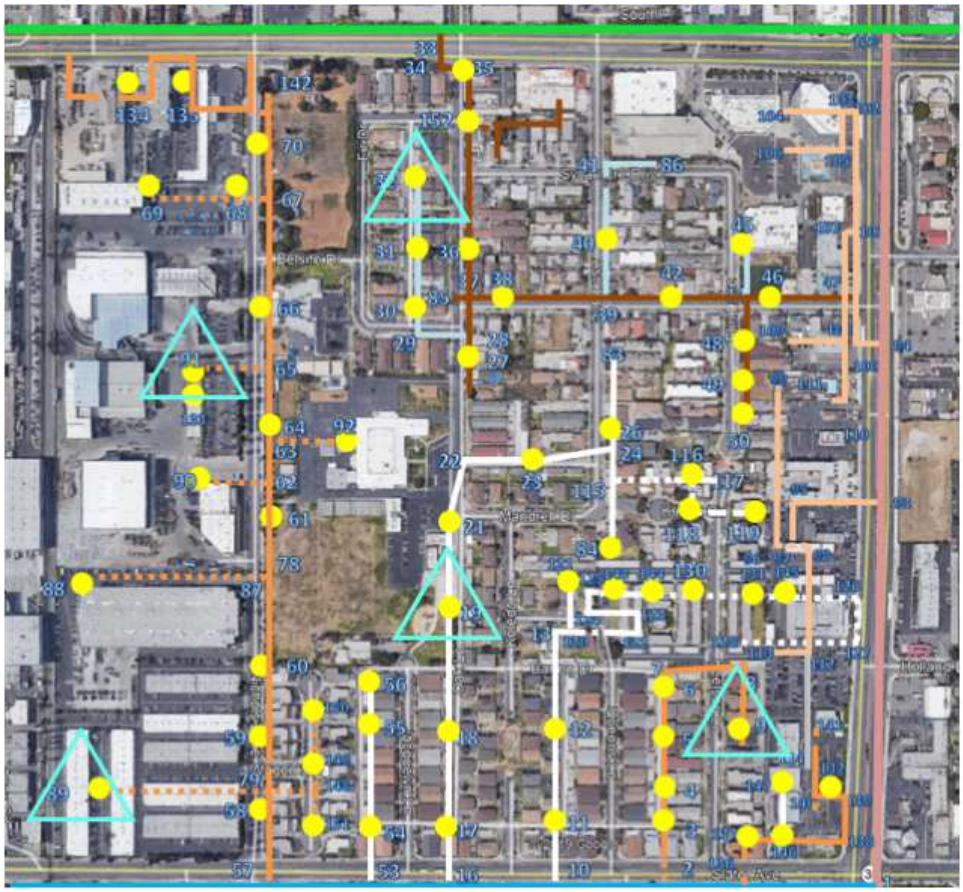

Figure 13 Selection of nodes that serves as growing points are marked in blue triangles. Note that although each islanded scenario has same starting points to form islands, the eventual island formation may differ as the imbalance between electric demand and supply changes.

The Baseline Scenario set is developed mainly for reference purpose to highlight how DER/ESS and EV impact the microgrid system and how resilient and reliable the microgrid system remains under islanded operation mode. Based on criteria developed in 6.4, selection of the starting point for each island for all scenarios under islanded operation mode is shown in Figure 13. Both grid connected and islanded operation mode were considered, where the former were considered both with no DER/ESS and with fixed DER/ESS in place whereas for the latter only when DER/ESS was in place.

6.5.2 MEDIUM PENETRATION EV SCENARIOS

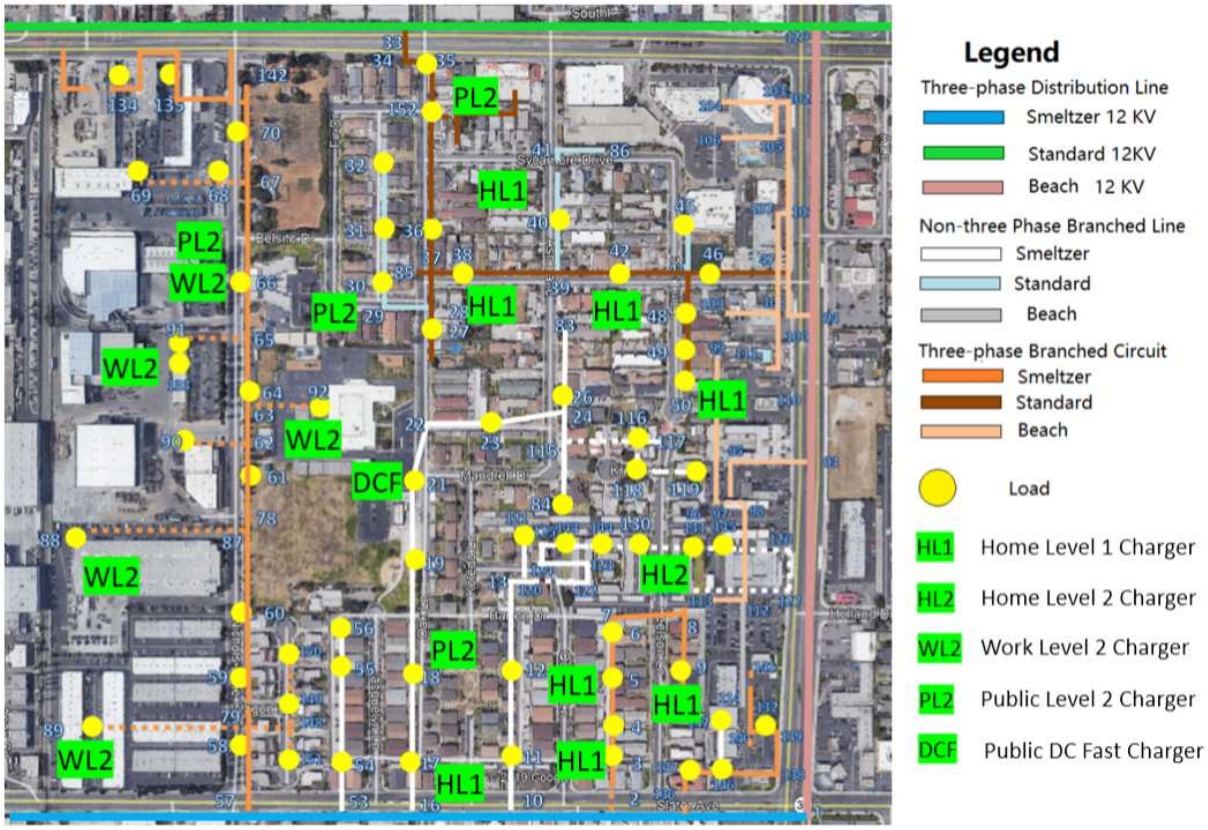

Figure 14 Selection of different types and levels of EV charging infrastructures. Locations and types of chargers are marked in green.

These scenarios were designed based on California Energy Commission's (CEC) projection of EV infrastructure projection to state's 2025 Zero-Emission-Vehicle deployment goals [65], and were materialized with different types of EV chargers. The total number of chargers and charging profiles of different types were determined by methods discussed in 6.2, while the locations to install chargers were determined by practical installation difficulty evaluated from site visits as well as building type, as shown in Figure 14. Both grid connected and islanded operation mode were considered, where the former were considered both with no DER/ESS operation and with fixed DER/ESS operation whereas the latter only when DER/ESS was in place.

6.5.3 HIGH PENETRATION EV SCENARIOS

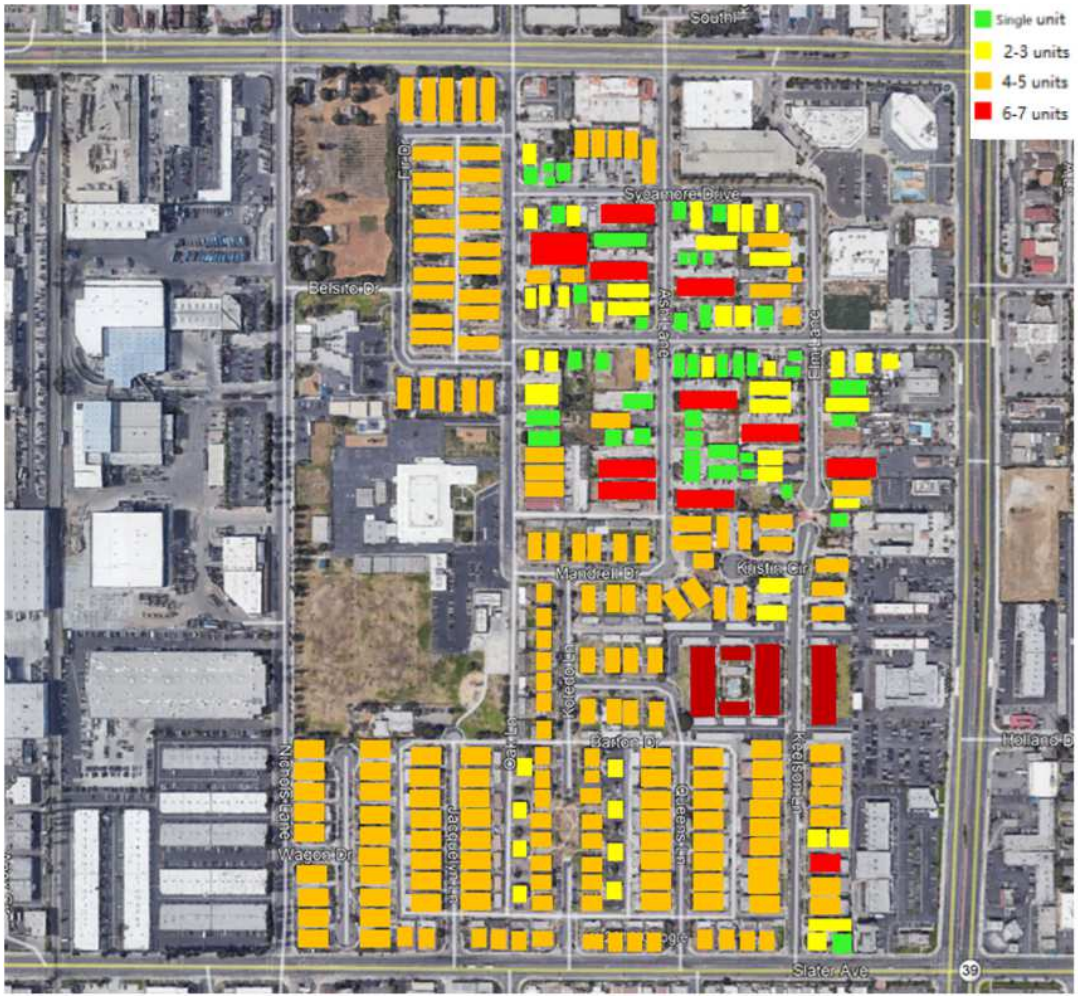

Figure 15 Residential unit density map of the Oak View Community

Scenarios under this category represent the ideal case where every utility customer own and charge one EV inside the community. Home Level 1 charging is considered to be the primary way of recharging all of EVs. Home level 1 chargers were deployed based upon residential unit density as shown in Figure 15. Other types of chargers were installed based on Figure 14. It was assumed that each residential unit has one Level 1 charger. In total, this scenario results in the addition of 318 Level 1 chargers to the examined AC Power Flow model. Both grid connected and islanded operation mode were considered, where the former was considered both with no DER/ESS operation and with fixed DER/ESS operation,

whereas for the latter only when DER/ESS is in place.

6.6 Static Result in OpenDSS

This section shows results from application of DER/ESS, EV adoption as well as the optimal topology design algorithm mentioned above to each scenario. Line-Neutral voltage results are presented to show either the impact of EV charging on electric power quality or that of DER/ESS or both together. A 5% deviation from standard voltage is considered acceptable [70] and lower and upper voltage limit were marked in results. Cable ampacity results and overload review of each scenario are presented to show the degree of electric pressure on basic electric infrastructures. Percent of overload calculated by ratio of peak load to transformer rating as well as overload frequency are also presented. Different ampacity ratings of electric conductor were also highlighted according to AWG [63]. Both voltage and ampacity results are demonstrated using box plots, where the x-axis of those figures indicates the start of branch circuits. Transformers and cables for each branch are shown in order of proximity to start of branch circuit. The middle red line in each box plot indicates the median annual value. the 25^{th} and 75^{th} percentile values are shown as the bottom and top of each box, respectively. All regular data falls within the whiskers and extreme data points as red '+' markers.

6.6.1 BASELINE SCENARIO RESULTS

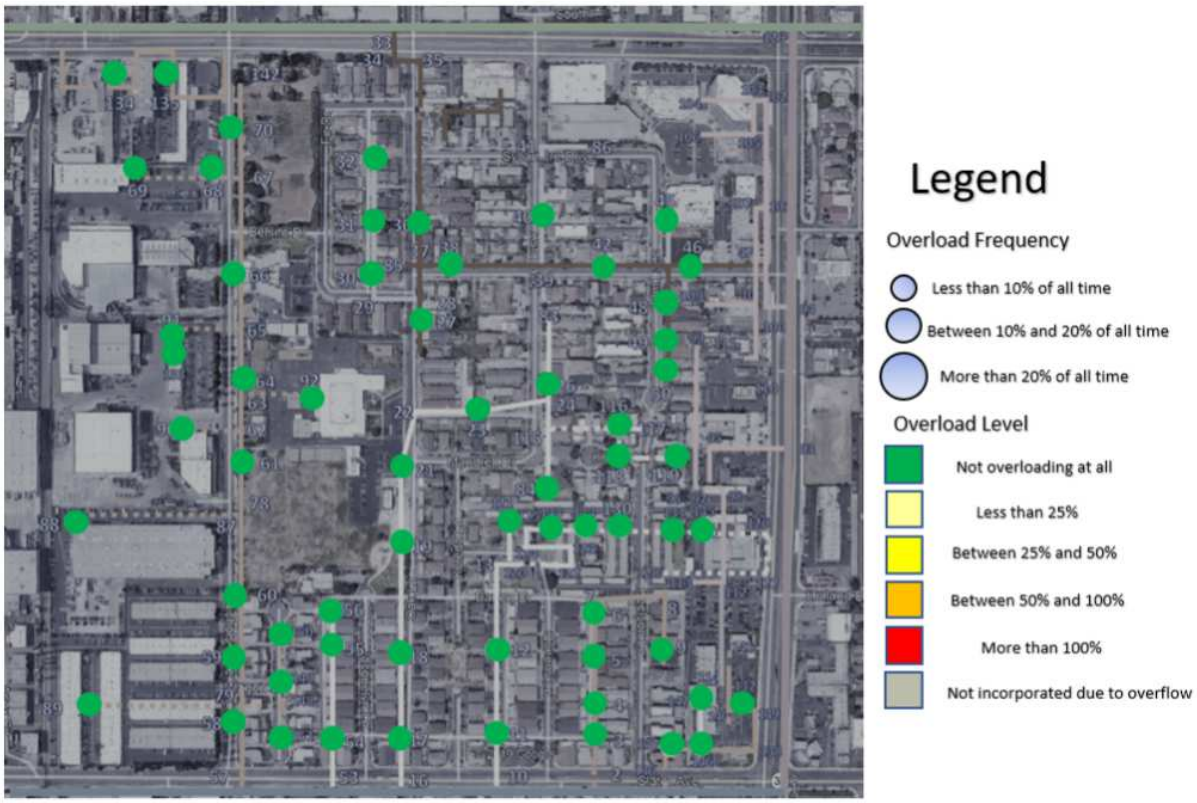

Figure 16 Overload situation of active transformers without DER/ESS in Baseline Scenario under grid connected mode

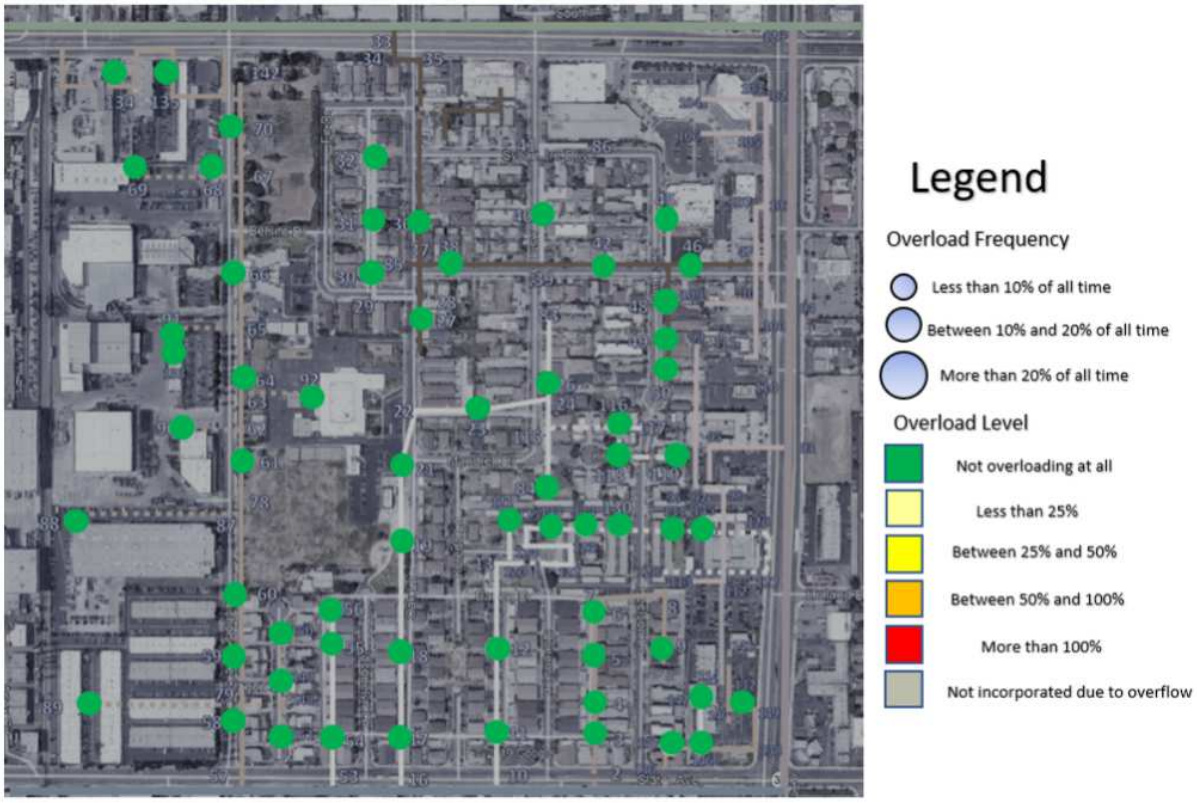

Figure 17 Overload situation of active transformers with DER/ESS in Baseline Scenario under grid connected mode

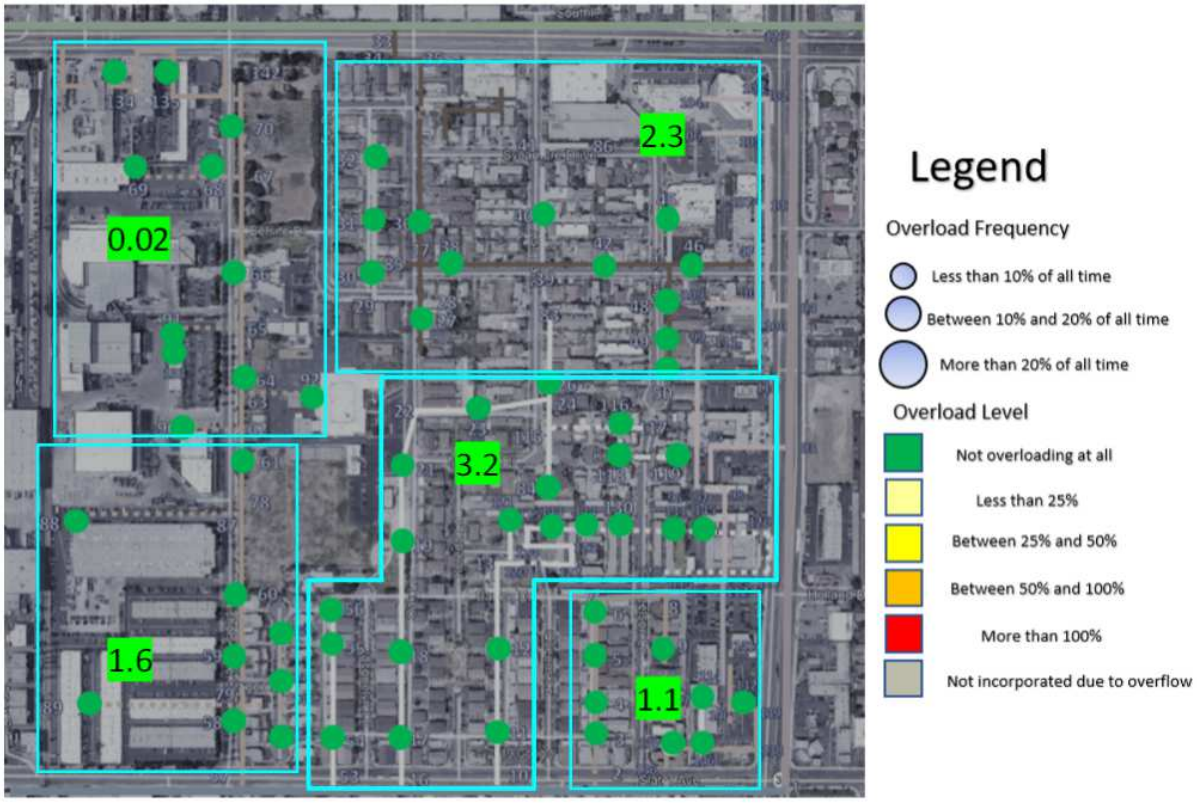

Figure 18 Overload situation of active transformers with DER/ESS in Baseline Scenario in island operation mode. Final results for the formation of each island are circled in blue. Numbers marked green represent the absolute difference in KW of each island's power supply and demand.

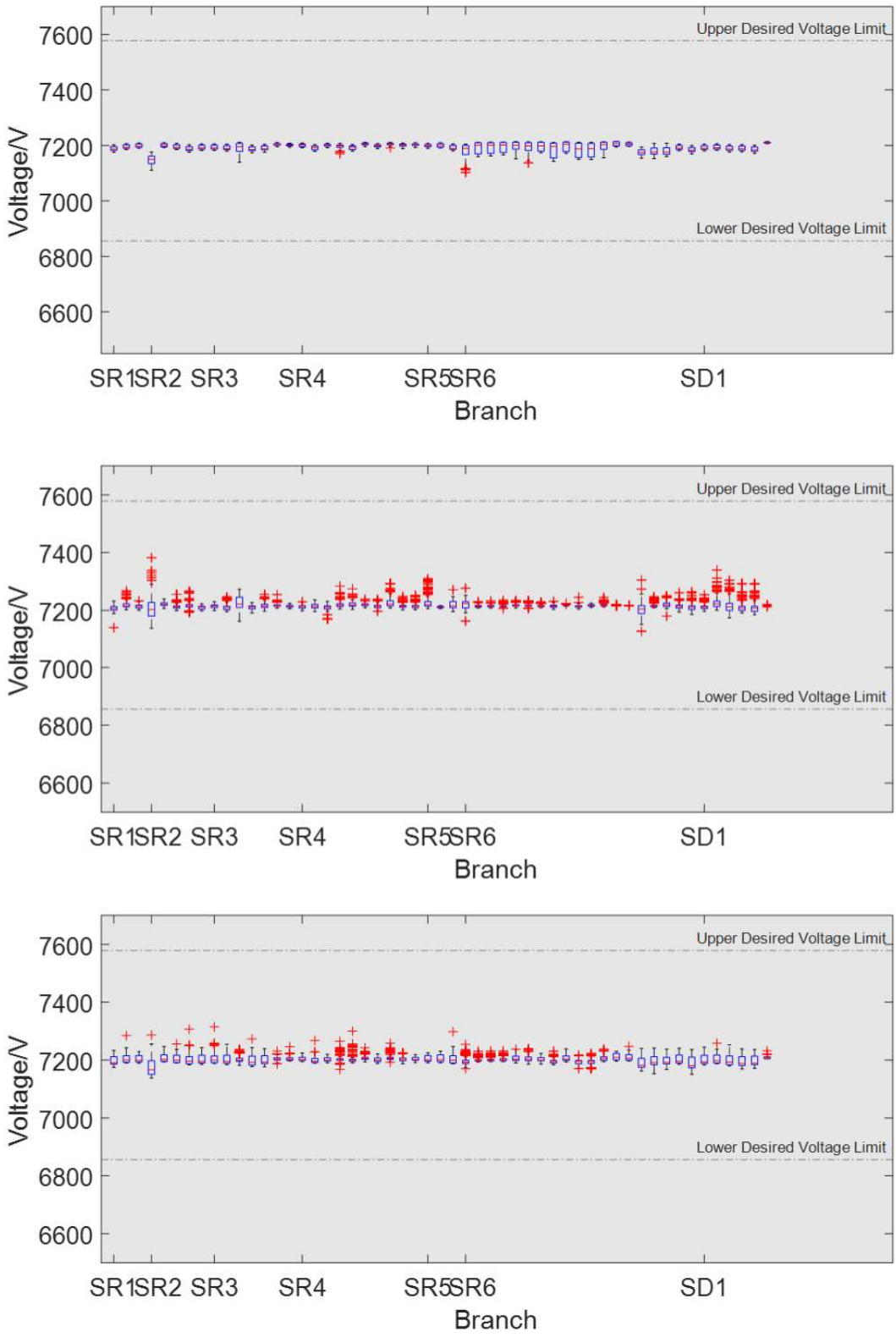

Figure 19 From top to bottom: Line-Neutral voltage of the Baseline Scenario, Baseline Scenario with DER/ESS, Baseline Scenario under islanded operation mode. Lower and upper

acceptable voltage limit are marked.

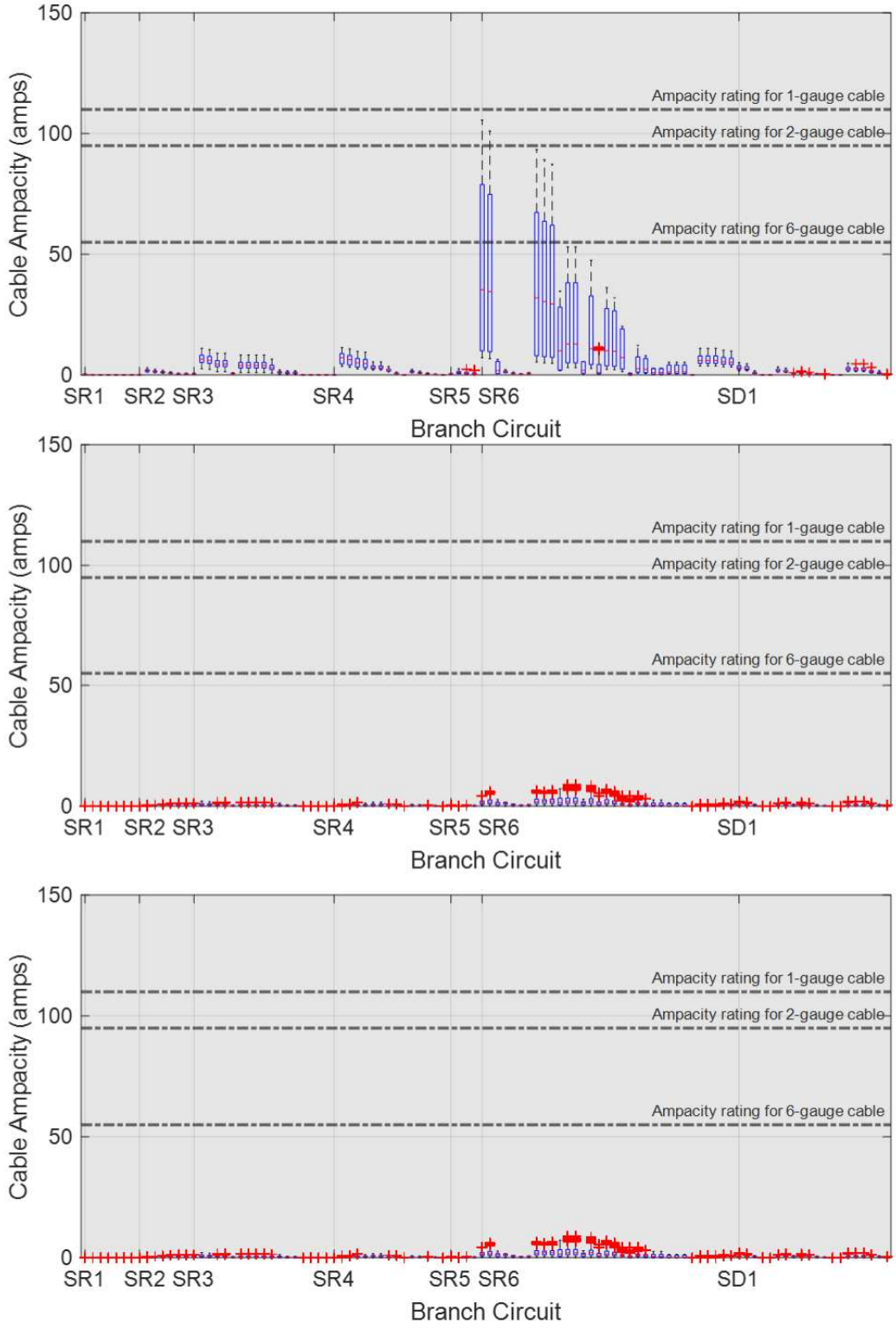

Figure 20 From top to bottom: Cable ampacity of the Baseline Scenario, Baseline Scenario with DER/ESS, Baseline Scenario under islanded operation mode. AWG ampacity ratings for

different gauged cables are marked.

Figure 16 and Figure 17 shows the overload state of active transformers in the Baseline Scenario without and with DER in place, respectively. No apparent overloading of transformers was found. **Error! Reference source not found.** indicates the overload state as well as power imbalance of each island in island operation mode in the same scenario. No apparent overloading of transformers was found either.

Figure 19 and Figure 20 illustrate the Line-Neutral voltage and cable ampacity of the Baseline Scenario, Baseline Scenario with active DER/ESS, Baseline Scenario under islanded operation mode. No breaching of voltage or ampacity rating limit was found for any of these scenarios.

6.6.2 MEDIUM PENETRATION EV SCENARIO RESULTS

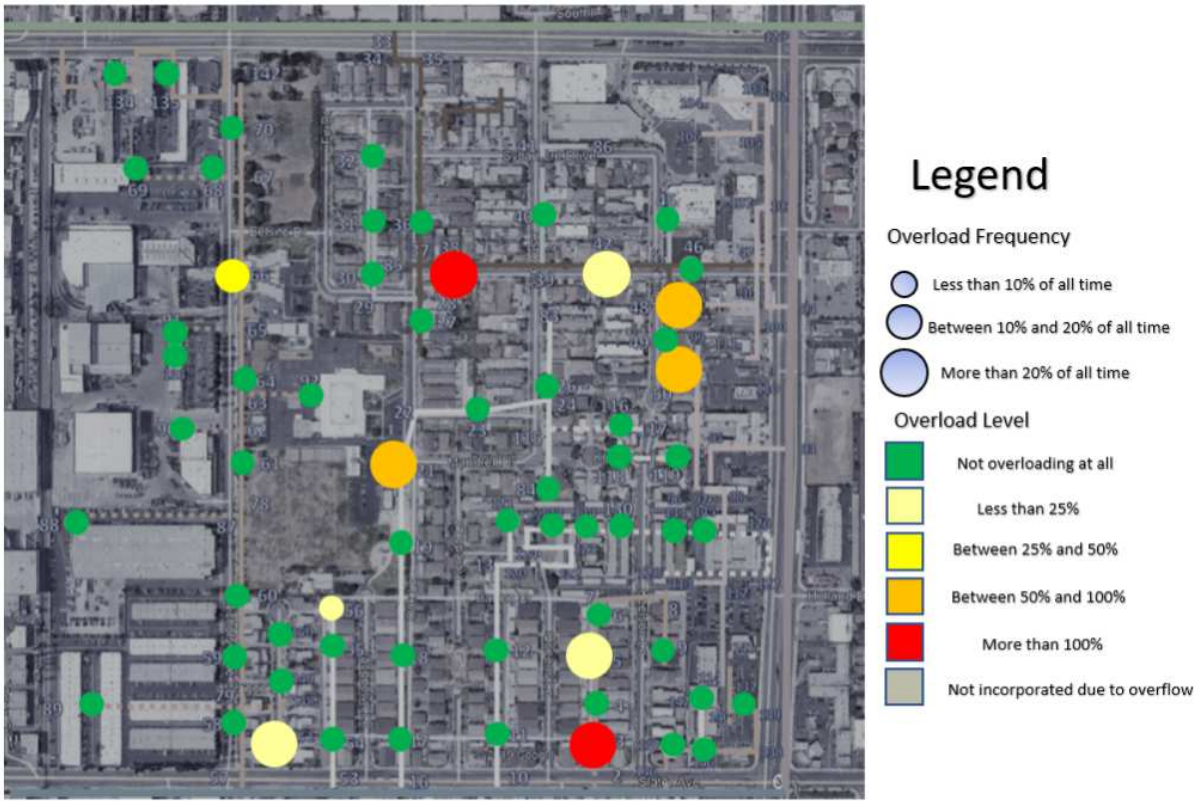

Figure 21 Overload situation of active transformers without DER/ESS in Medium Penetration

EV Scenario under grid connected mode

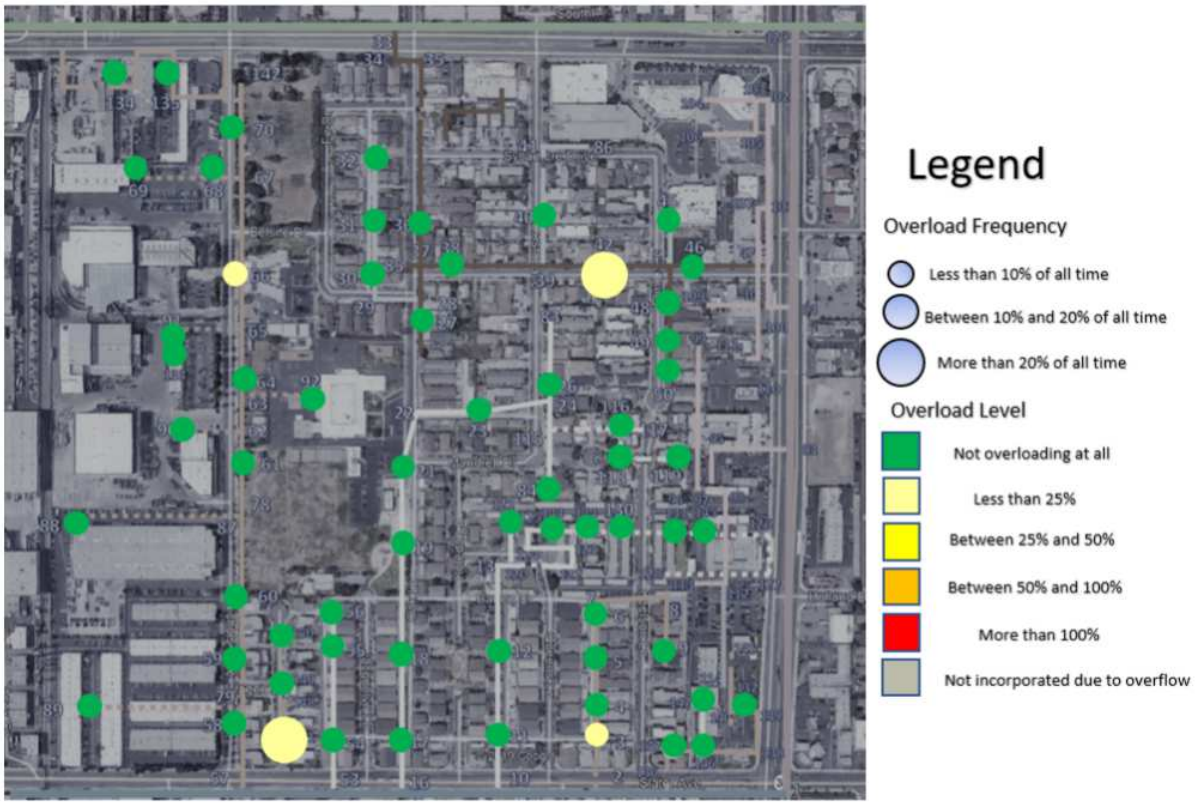

Figure 22 Overload situation of active transformers with DER/ESS in Medium Penetration EV Scenario under grid connected mode

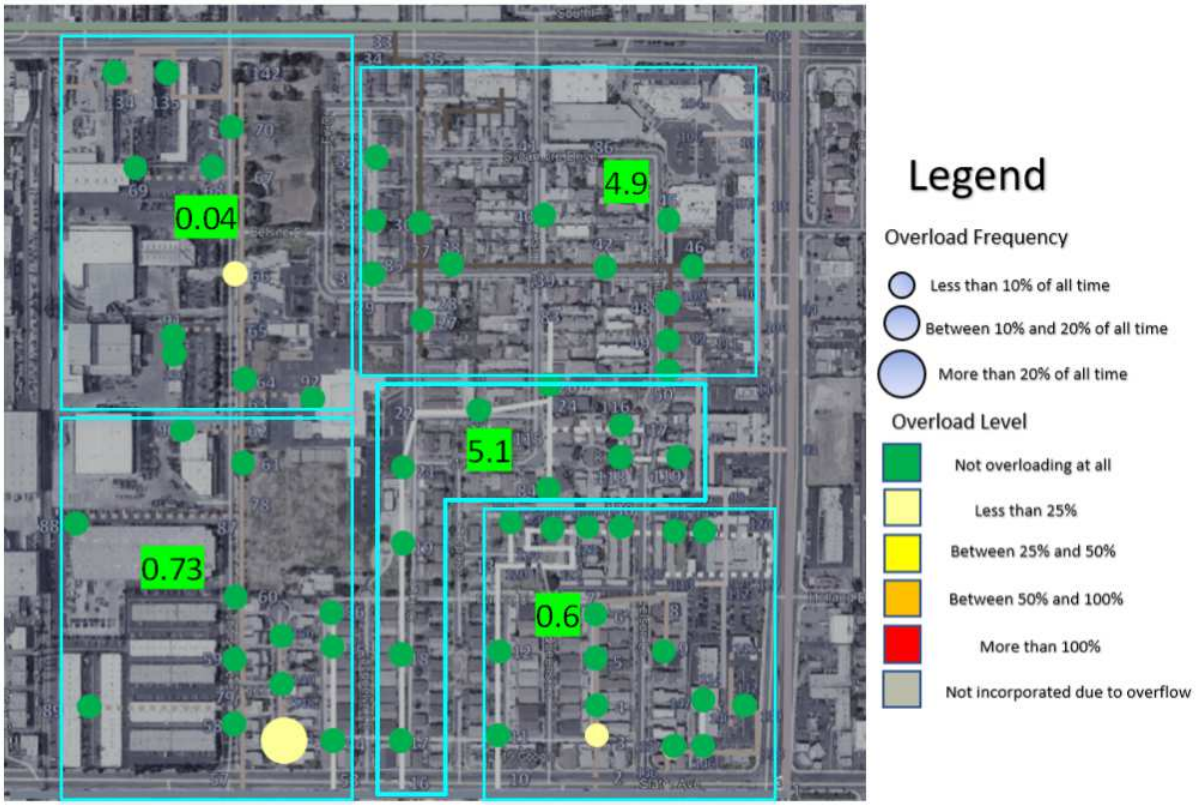

Figure 23 Overload situation of active transformers with DER/ESS in Medium Penetration EV Scenario in island operation mode. Final results for the formation of each island are circled in blue. Numbers marked green represent the absolute difference in KW of each island's power supply and demand.

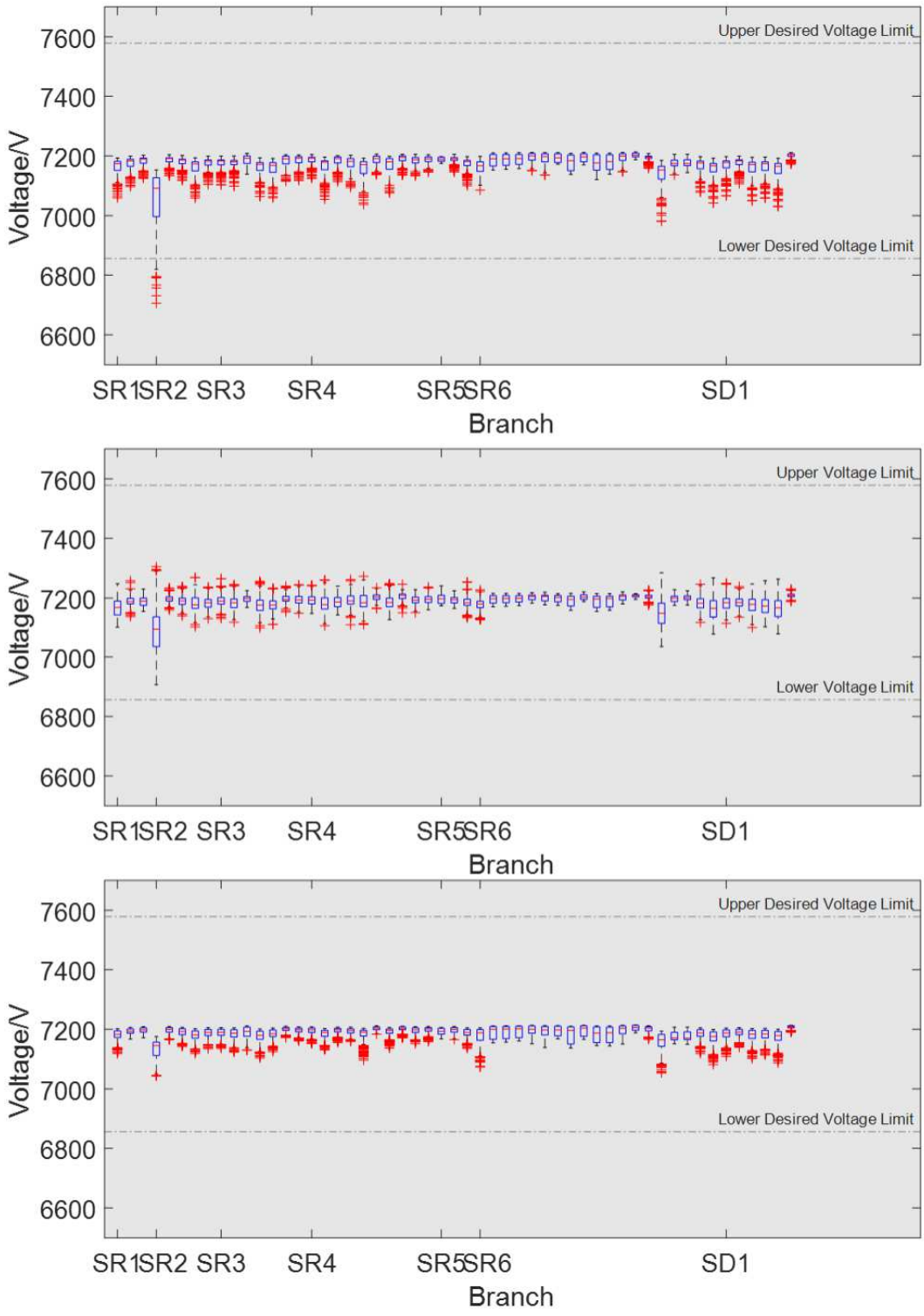

Figure 24 From top to bottom: Line-Neutral voltage of the Medium Penetration EV Scenario under normal operation mode, normal operation mode with DER/ESS, island operation mode

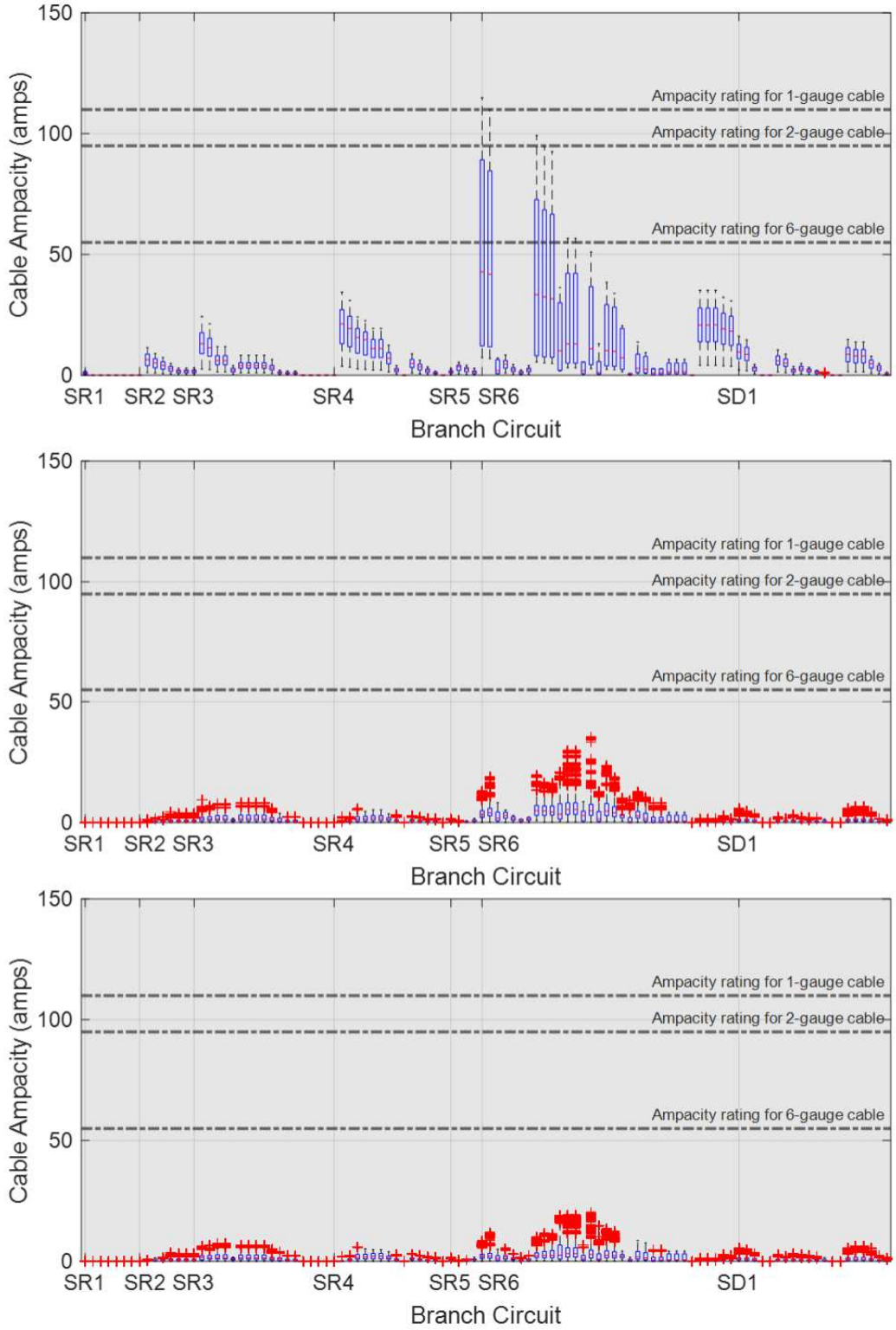

Figure 25 From top to bottom: Cable ampacity of the Medium Penetration EV Scenario under normal operation mode, normal operation mode with DER/ESS, island operation mode

Figure 21 shows the overload state of active transformers in able to meeting CA 2025 ZEV goal [65] , without and with DER in place respectively. Nine transformers were found to have overloading issues, two of which were severe in degree, when no DER/ESS was applied in normal operation mode. After the application of DER/ESS, however, the severeness of the overloading problem was greatly curbed, as described in Figure 22. Figure 23 indicates the overload state as well as power imbalance of each island in island operation mode in the same scenario. Although overloading problem still existed, the overall degree and frequency have been greatly reduced compared to Figure 21, and was also slightly better than that with same level of DER/ESS in grid connected operation mode as shown in Figure 22. The comparison shows the advantage of the optimal topology design algorithm of being able to further balance local power demand and supply.

Figure 24 and Figure 25 show the Line-Neutral voltage and cable ampacity of Medium Penetration EV Scenario, the same scenario with active DER/ESS, under islanded operation mode respectively. During normal operation mode with no DER/ESS, S2 on SR2 was shown to have the low voltage issue. Although other transformers were not found to have lower voltage outliers on par with S2, many of them, especially those on SR6, have shown the tendency to decrease to a lower voltage in case of high electric load. A one-off high ampacity outlier in Figure 25 at the very beginning of SR6 was believed to suffer from over ampacity issue. Although it may not cause an immediate cable failure, it is possible that a cautious and liability-conscious utility company or local electric system operator may turn to replace and upgrade that very cable segment or even the entire branch circuit due to practical engineer difficulty. With the enacting of DER/ESS, no voltage or ampacity issues were found again, with or without implementing optimal topology design for island formation. Still, it is clear that in island operation mode the DER/ESS was better harnessed as evidenced by a

smaller overall cable ampacity of island operation mode against normal operation mode in Figure 25.

6.6.3 HIGH PENETRATION EV SCENARIO RESULTS

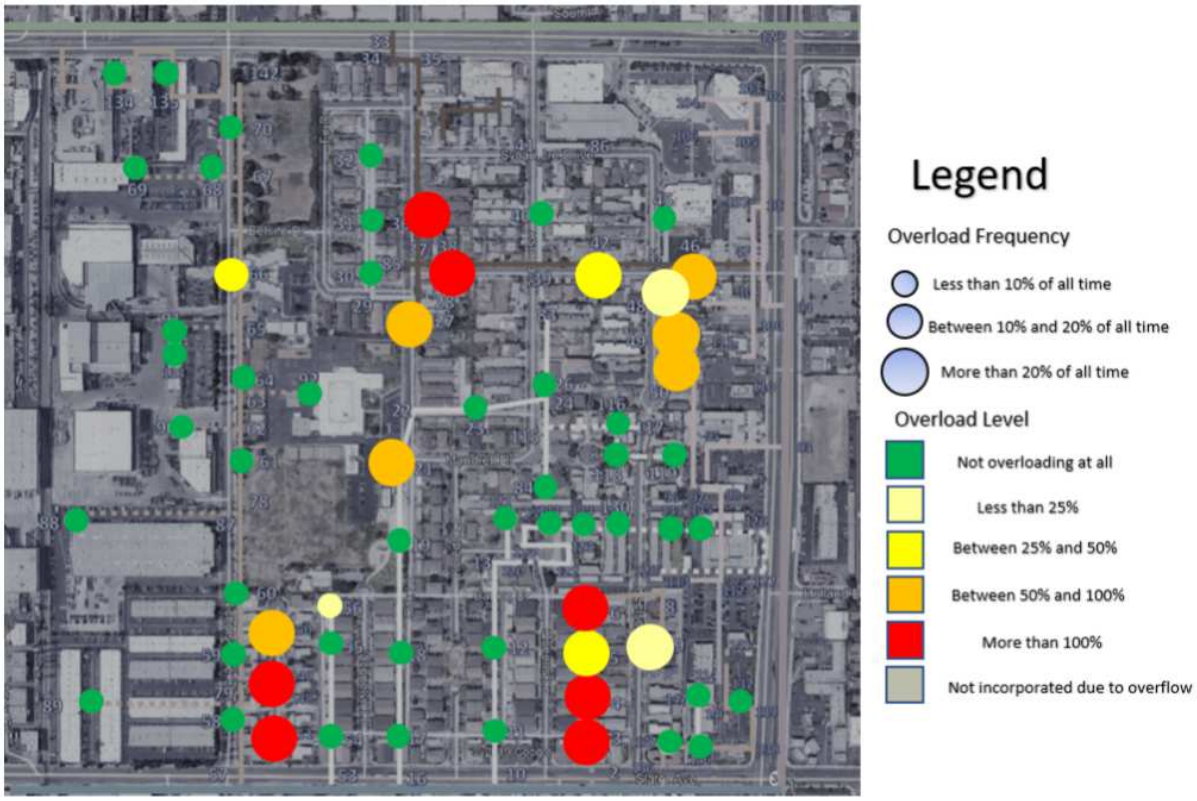

Figure 26 Overload situation of active transformers without DER/ESS in High Penetration EV Scenario under grid connected mode

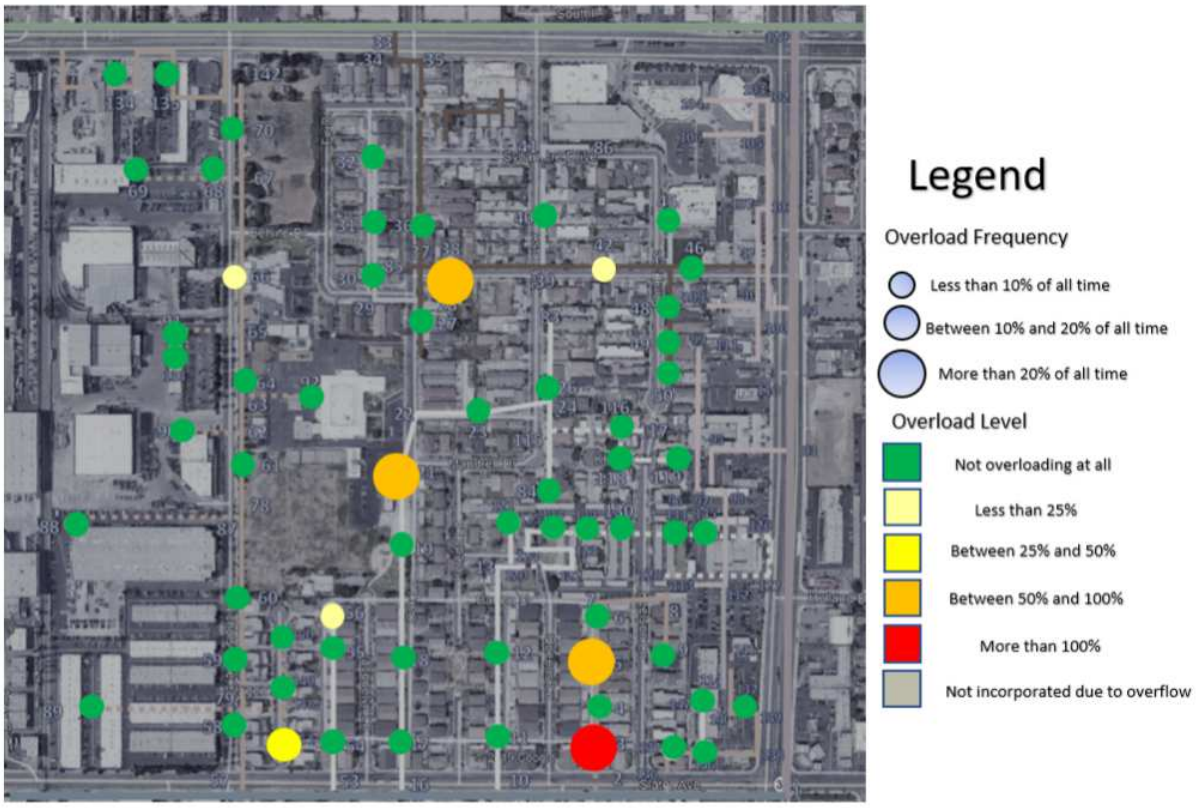

Figure 27 Overload situation of active transformers with DER/ESS in High Penetration EV Scenario under grid connected mode

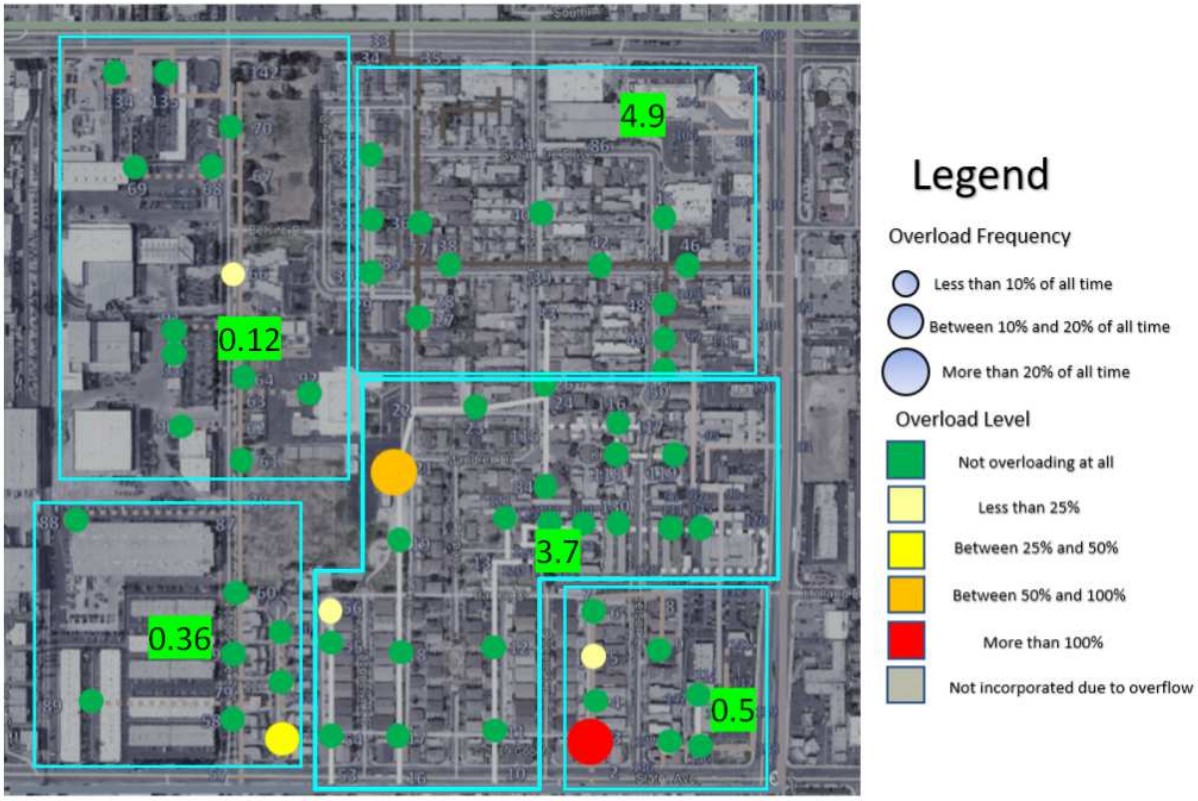

Figure 28 Overload situation of active transformers with DER/ESS in High Penetration EV Scenario in islanded operation mode. Final results for the formation of each island are circled in blue. Numbers marked green represent the absolute difference in KW of each island's power supply and demand.

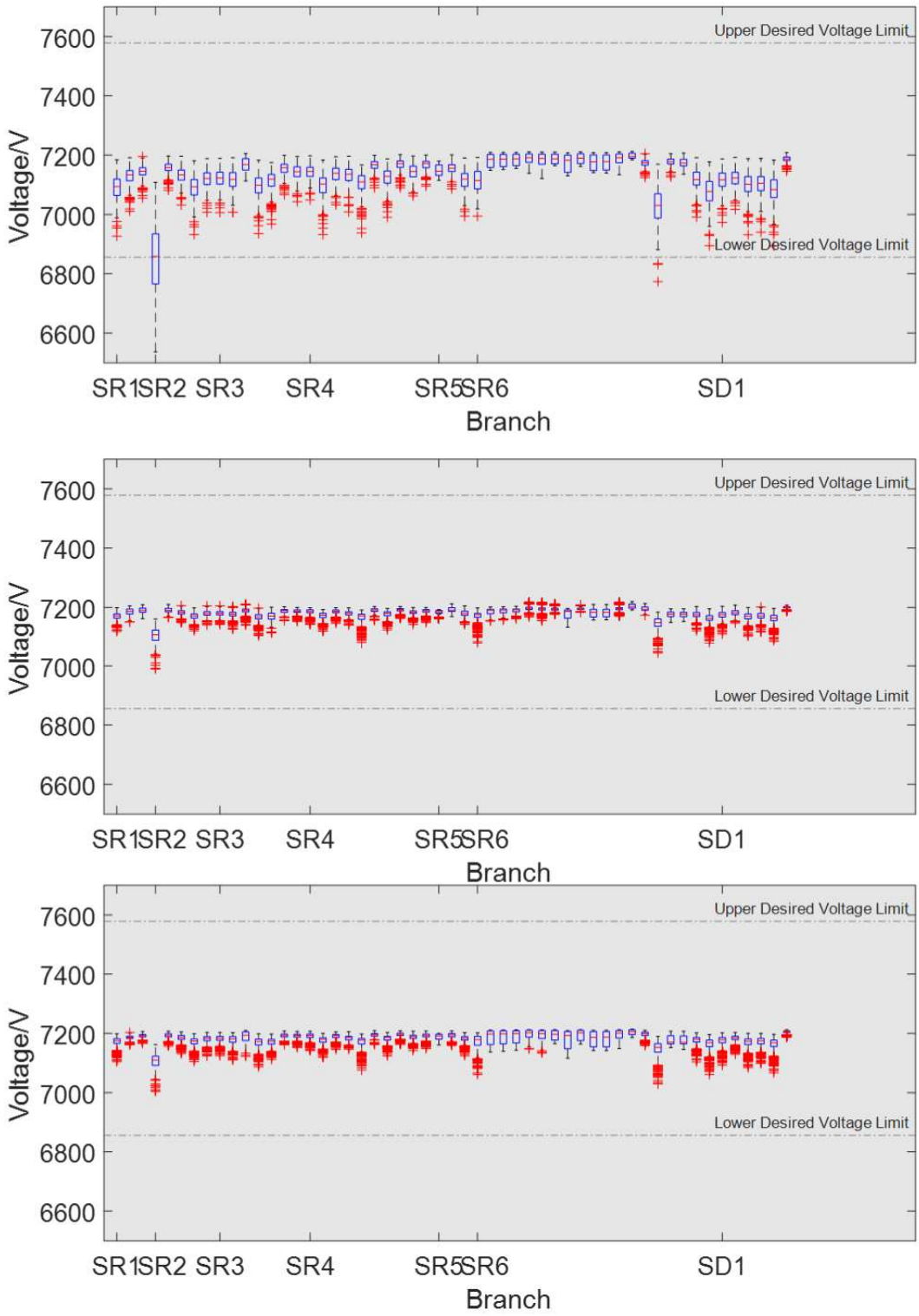

Figure 29 From top to bottom: Line-Neutral voltage of the High Penetration EV Scenario, High Penetration EV Scenario with DER/ESS, High Penetration EV Scenario under islanded operation mode. Lower and upper acceptable voltage limit are marked.

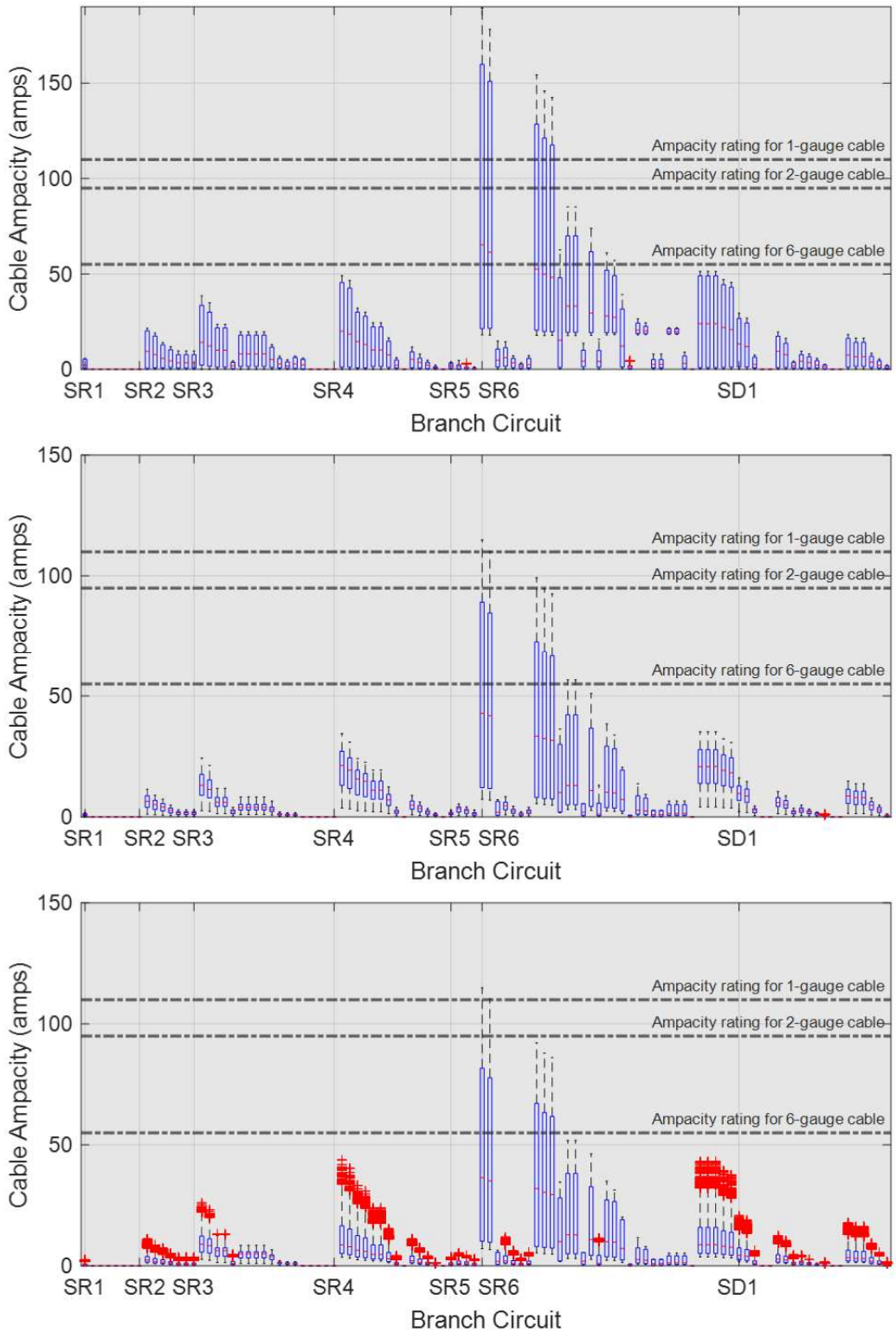

Figure 30 From top to bottom: Cable ampacity of the High Penetration EV Scenario, High Penetration EV Scenario with DER/ESS, High Penetration EV Scenario under islanded operation mode. AWG ampacity ratings for different gauged cables are marked.

Figure 26Figure 16 and Figure 27 show the overload state of active transformers in the case where 100% conversion to EV using Level 1 chargers happened, without and with DER in place, respectively. A shocking percentage of about 40% of total active transformers were found to have different levels of overloading problem, with 1/3 of them in extreme degree when DER/ESS was not active. A catastrophic grid failure would most likely happen from the overloading. Figure 28 indicates the overload state as well as power imbalance of each island in island operation mode in the same scenario. Although a certain degree of overloading still exists in various transformers, it is believed that better power balance within islands resulted in a reduced degree of the problem compared to that of the same scenario when DER/ESS was installed.

Figure 29 and Figure 30 show the Line-Neutral voltage and cable ampacity of High Penetration EV Scenario, the same scenario with active DER/ESS, under islanded operation mode respectively. During normal operation mode with no DER/ESS, two transformers on SR2 and SD6 were diagnosed with low voltage issues. Also, it is worth pointing out that the average voltage for all active transformers dropped 1.5% in the same scenario. Significant breaching of ampacity rating on the beginning of SR6 was found and could most likely result in a cable failure that may shut down the power supply of the entire branch circuit. Once again, with DER/ESS in place, no voltage or ampacity issues were found again, in both grid connected mode and islanded operation mode. The average voltage under these two scenarios, though still slightly below the desired 7.2 KV level, is well accepted. Once again it shows that in islanded operation mode the optimal topology design algorithm worked and the outperformed installing DER/ESS in grid connected scenario in terms of electric power quality.

7 Summary and Conclusions

In this thesis, a two-stage Graph Partitioning and MILP algorithm-based microgrid topology design applicable to radial grids was demonstrated, after a thorough literature review was done, a real-life based OpenDSS community topology model was developed, and different levels of EV load and charger count were estimated for future work.

The accuracy of DERopt Baseline dynamics were then verified by E3 RESOLVE model using same inputs to ensure accuracy of DERopt AC Power Flow model accuracy and similar energy dynamic results of same level were found. DERopt power dynamics were crucial to future analysis.

The effectiveness of DER/ESS and the proposed microgrid topology optimization method was further verified in OpenDSS using 9 examples based on the AC Power Flow model of the very community with overload report and static electric results represented by Line-Neutral voltage and cable ampacity in boxplots.

Results show that without DER/ESS, a high penetration of EV adoption in the community would crash a large percentage of local electric infrastructure including distribution transformers and power cables, and upgrade is needed for both. In the most extreme scenario, 40% of total active transformers would have to deal with overloading problem and about 28% of them will likely stop function very soon due to an extreme degree and long durance of operating well above standard capacity.

It is also shown that to either meet the requirement of CA 2025 State ZEV goal or to fully convert the community vehicles to EVs, power quality will be disturbed and the lifespan of domestic electric appliance operating in long duration under the estimated lower voltage

may be negatively impacted.

It is also shown that the addition of DER/ESS without changing grid operating mode can in many cases mitigate the overloading and power quality issues, but under islanded operation mode with optimally designed islands a better overall balance of power demand and supply was always achieved. Therefore, it is believed that the design and operation of DER/ESS works, and the studied island topology design algorithm works better to provide the community with resilient and reliable energy solution.

It is also worth pointing out that in both operation modes no evidence was found that the addition of DER/ESS causes voltage issues from power backflow. This conclusion inspires and encourages the author to further increase DER penetration level into the community to convert the community to 100% renewable energy usage.

References

[1] Ayub M, Gan CK, Kadir AFA. The impact of grid-connected PV systems on Harmonic Distortion. 2014 IEEE Innov Smart Grid Technol - Asia, ISGT ASIA 2014 2014:669–74. https://doi.org/10.1109/ISGT-Asia.2014.6873872.

[2] Uddin M, Romlie MF, Abdullah MF, Abd Halim S, Abu Bakar AH, Chia Kwang T. A review on peak load shaving strategies. Renew Sustain Energy Rev 2018;82:3323–32. https://doi.org/10.1016/j.rser.2017.10.056.

[3] Drude L, Pereira Junior LC, Rüther R. Photovoltaics (PV) and electric vehicle-to-grid (V2G) strategies for peak demand reduction in urban regions in Brazil in a smart grid environment. Renew Energy 2014;68:443–51. https://doi.org/10.1016/j.renene.2014.01.049.

[4] Kisacikoglu MC, Kesler M, Tolbert LM. Single-phase on-board bidirectional PEV charger for V2G reactive power operation. IEEE Trans Smart Grid 2015;6:767–75. https://doi.org/10.1109/TSG.2014.2360685.

[5] Mets K, Verschueren T, De Turck F, Develder C. Exploiting V2G to optimize residential energy consumption with electrical vehicle (dis)charging. 2011 IEEE 1st Int Work Smart Grid Model Simulation, SGMS 2011 2011:7–12. https://doi.org/10.1109/SGMS.2011.6089203.

[6] Erol-Kantarci M, Kantarci B, Mouftah HT. Reliable overlay topology design for the smart microgrid network. IEEE Netw 2011. https://doi.org/10.1109/MNET.2011.6033034.

[7] Jiménez-Fernández S, Camacho-Gómez C, Mallol-Poyato R, Fernández JC, Del Ser J, Portilla-Figueras A, et al. Optimal microgrid topology design and siting of distributed generation sources using a multi-objective substrate Layer Coral Reefs Optimization Algorithm. Sustain 2018. https://doi.org/10.3390/su11010169.

[8] Talukdar S, Deka D, Materassi D, Salapaka M. Exact topology reconstruction of radial dynamical systems with applications to distribution system of the power grid. Proc. Am. Control Conf., 2017. https://doi.org/10.23919/ACC.2017.7963053.

[9] CORP IH. ABOUT THE NATIONAL POWER GRID n.d. https://www.itc-holdings.com/a-modern-power-grid/about-the-national-power-grid.

[10] Edison Tech Center. The History of Electrification n.d. https://edisontechcenter.org/HistElectPowTrans.html.

[11] Momoh JA. Smart grid design for efficient and flexible power networks operation and control. 2009 IEEE/PES Power Syst Conf Expo PSCE 2009 2009. https://doi.org/10.1109/PSCE.2009.4840074.

[12] GUARNIERI M, Liserre M, Sauter T, Hung JY. Future energy systems: Integrating

renewable energy sources into the smart power grid through industrial electronics. IEEE Ind Electron Mag 2010;4:18–37. https://doi.org/10.1109/MIE.2010.935861.

[13] Ito T, Miyata H, Taniguchi M, Aihara T, Uchiyama N, Konishi H. Harmonic current reduction control for grid-connected PV generation systems. 2010 Int Power Electron Conf - ECCE Asia -, IPEC 2010 2010:1695–700. https://doi.org/10.1109/IPEC.2010.5542128.

[14] Castilla M, Miret J, Camacho A, Matas J, De Vicuna LG. Reduction of current harmonic distortion in three-phase grid-connected photovoltaic inverters via resonant current control. IEEE Trans Ind Electron 2013;60:1464–72. https://doi.org/10.1109/TIE.2011.2167734.

[15] ZEV Action Plan History n.d. https://business.ca.gov/industries/zero-emission-vehicles/zev-action-plan/.

[16] Wikipedia. Vehicle-to-grid n.d.

[17] Lund H, Kempton W. Integration of renewable energy into the transport and electricity sectors through V2G. Energy Policy 2008;36:3578–87. https://doi.org/10.1016/j.enpol.2008.06.007.

[18] Kempton W, Udo V, Huber K, Komara K, Letendre S, Baker S, et al. A Test of Vehicle-to-Grid (V2G) for Energy Storage and Frequency Regulation in the PJM System 2008;2008.

[19] Bishop JDK, Axon CJ, Bonilla D, Tran M, Banister D, McCulloch MD. Evaluating the impact of V2G services on the degradation of batteries in PHEV and EV. Appl Energy 2013;111:206–18. https://doi.org/10.1016/j.apenergy.2013.04.094.

[20] Yilmaz M, Krein PT. Review of benefits and challenges of vehicle-to-grid technology. 2012 IEEE Energy Convers Congr Expo ECCE 2012 2012:3082–9. https://doi.org/10.1109/ECCE.2012.6342356.

[21] Li W, Joós G. Comparison of energy storage system technologies and configurations in a wind farm. PESC Rec - IEEE Annu Power Electron Spec Conf 2007:1280–5. https://doi.org/10.1109/PESC.2007.4342177.

[22] Qin J, Han X, Liu G, Wang S, Li W, Jiang Z. Wind and Storage Cooperative Scheduling Strategy Based on Deep Reinforcement Learning Algorithm. J Phys Conf Ser 2019;1213. https://doi.org/10.1088/1742-6596/1213/3/032002.

[23] Zhao H, Wu Q, Hu S, Xu H, Rasmussen CN. Review of energy storage system for wind power integration support. Appl Energy 2015;137:545–53. https://doi.org/10.1016/j.apenergy.2014.04.103.

[24] Bahramirad S, Reder W, Khodaei A. Reliability-constrained optimal sizing of energy storage system in a microgrid. IEEE Trans Smart Grid 2012;3:2056–62. https://doi.org/10.1109/TSG.2012.2217991.

[25] Chen C, Duan S, Cai T, Liu B, Hu G. Smart energy management system for optimal microgrid economic operation. IET Renew Power Gener 2011;5:258–67. https://doi.org/10.1049/iet-rpg.2010.0052.

[26] Chen C, Duan S. Optimal allocation of distributed generation and energy storage

system in microgrids. IET Renew Power Gener 2014;8:581–9. https://doi.org/10.1049/iet-rpg.2013.0193.

[27] Marnay C, Bailey OC. The CERTS microgrid and the future of the macrogrid. Public Interest 2004.

[28] Talei H, Zizi B, Abid MR, Essaaidi M, Benhaddou D, Khalil N. Smart campus microgrid: Advantages and the main architectural components. Proc 2015 IEEE Int Renew Sustain Energy Conf IRSEC 2015 2016. https://doi.org/10.1109/IRSEC.2015.7455093.

[29] Distributed generation n.d. https://doi.org/https://en.wikipedia.org/wiki/Distributed_generation.

[30] Flores RJ, Brouwer J. Optimal design of a distributed energy resource system that economically reduces carbon emissions. Appl Energy 2018;232:119–38. https://doi.org/10.1016/j.apenergy.2018.09.029.

[31] Pudjianto D, Ramsay C, Strbac G. Virtual power plant and system integration of distributed energy resources. IET Renew Power Gener 2008;2:228–38. https://doi.org/10.1049/iet-rpg:20070106.

[32] Kardakos EG, Simoglou CK, Bakirtzis AG. Optimal Offering Strategy of a Virtual Power Plant: A Stochastic Bi-Level Approach. IEEE Trans Smart Grid 2016;7:794–806. https://doi.org/10.1109/TSG.2015.2419714.

[33] Domingo CM. RNM: Reference Network Model n.d. https://www.iit.comillas.edu/technology-offer/rnm.

[34] Novoa L, Flores R, Brouwer J. Optimal renewable generation and battery storage sizing and siting considering local transformer limits. Appl Energy 2019;256:113926. https://doi.org/10.1016/j.apenergy.2019.113926.

[35] Xu Y, Zhang W, Hug G, Kar S, Li Z. Cooperative control of distributed energy storage systems in a microgrid. IEEE Trans Smart Grid 2015. https://doi.org/10.1109/TSG.2014.2354033.

[36] Dorfler F, Simpson-Porco JW, Bullo F. Breaking the hierarchy: Distributed control and economic optimality in Microgrids. IEEE Trans Control Netw Syst 2016. https://doi.org/10.1109/TCNS.2015.2459391.

[37] Parisio A, Rikos E, Glielmo L. A model predictive control approach to microgrid operation optimization. IEEE Trans Control Syst Technol 2014. https://doi.org/10.1109/TCST.2013.2295737.

[38] Che L, Zhang X, Shahidehpour M, Alabdulwahab A, Al-Turki Y. Optimal Planning of Loop-Based Microgrid Topology. IEEE Trans Smart Grid 2017. https://doi.org/10.1109/TSG.2015.2508058.

[39] Cortes CA, Contreras SF, Shahidehpour M. Microgrid topology planning for enhancing the reliability of active distribution networks. IEEE Trans Smart Grid 2018. https://doi.org/10.1109/TSG.2017.2709699.

[40] Arefifar SA, Mohamed YARI, El-Fouly THM. Optimum microgrid design for enhancing reliability and supply-security. IEEE Trans Smart Grid 2013.

https://doi.org/10.1109/TSG.2013.2259854.

[41] Gazijahani FS, Salehi J. Robust Design of Microgrids with Reconfigurable Topology under Severe Uncertainty. IEEE Trans Sustain Energy 2018. https://doi.org/10.1109/TSTE.2017.2748882.

[42] Kirthiga MV, Daniel SA, Gurunathan S. A methodology for transforming an existing distribution network into a sustainable autonomous micro-grid. IEEE Trans Sustain Energy 2013. https://doi.org/10.1109/TSTE.2012.2196771.

[43] Sechilariu M, Wang BC, Locment F. Supervision control for optimal energy cost management in DC microgrid: Design and simulation. Int J Electr Power Energy Syst 2014. https://doi.org/10.1016/j.ijepes.2014.01.018.

[44] Nguyen DT, Le LB. Risk-constrained profit maximization for microgrid aggregators with demand response. IEEE Trans Smart Grid 2015. https://doi.org/10.1109/TSG.2014.2346024.

[45] Gazijahani FS, Salehi J. Game Theory Based Profit Maximization Model for Microgrid Aggregators with Presence of EDRP Using Information Gap Decision Theory. IEEE Syst J 2019. https://doi.org/10.1109/JSYST.2018.2864578.

[46] Tsao YC, Thanh V Van. Toward blockchain-based renewable energy microgrid design considering default risk and demand uncertainty. Renew Energy 2021. https://doi.org/10.1016/j.renene.2020.09.016.

[47] Qin M, Chan KW, Chung CY, Luo X, Wu T. Optimal planning and operation of energy storage systems in radial networks for wind power integration with reserve support. IET Gener Transm Distrib 2016. https://doi.org/10.1049/iet-gtd.2015.1039.

[48] Dou C, Yue D, Guerrero JM, Xie X, Hu S. Multiagent System-Based Distributed Coordinated Control for Radial DC Microgrid Considering Transmission Time Delays. IEEE Trans Smart Grid 2017. https://doi.org/10.1109/TSG.2016.2524688.

[49] Almadhor A. Feedback-Oriented Intelligent Monitoring of a Storage-Based Solar Photovoltaic (PV)-Powered Microgrid with Mesh Networks. Energies 2018;11:1446. https://doi.org/10.3390/en11061446.

[50] Trivedi A, Singh M. L1 Adaptive Droop Control for AC Microgrid with Small Mesh Network. IEEE Trans Ind Electron 2018. https://doi.org/10.1109/TIE.2017.2772211.

[51] Lou G, Gu W, Wang J, Sheng W, Sun L. Optimal Design for Distributed Secondary Voltage Control in Islanded Microgrids: Communication Topology and Controller. IEEE Trans Power Syst 2019. https://doi.org/10.1109/TPWRS.2018.2870058.

[52] Simpson-Porco JW, Shafiee Q, Dorfler F, Vasquez JC, Guerrero JM, Bullo F. Secondary Frequency and Voltage Control of Islanded Microgrids via Distributed Averaging. IEEE Trans Ind Electron 2015. https://doi.org/10.1109/TIE.2015.2436879.

[53] Ashabani SM, Mohamed YARI. A flexible control strategy for grid-connected and islanded microgrids with enhanced stability using nonlinear microgrid stabilizer. IEEE Trans Smart Grid 2012. https://doi.org/10.1109/TSG.2012.2202131.

[54] Etemadi AH, Davison EJ, Iravani R. A generalized decentralized robust control of islanded microgrids. IEEE Trans Power Syst 2014.

https://doi.org/10.1109/TPWRS.2014.2312615.

[55] Hossain MJ, Mahmud MA, Milano F, Bacha S, Hably A. Design of Robust Distributed Control for Interconnected Microgrids. IEEE Trans Smart Grid 2016. https://doi.org/10.1109/TSG.2015.2502618.

[56] Chen YK, Wu YC, Song CC, Chen YS. Design and implementation of energy management system with fuzzy control for DC microgrid systems. IEEE Trans Power Electron 2013. https://doi.org/10.1109/TPEL.2012.2210446.

[57] Kumar M, Singh SN, Srivastava SC. Design and control of smart DC microgrid for integration of renewable energy sources. IEEE Power Energy Soc. Gen. Meet., 2012. https://doi.org/10.1109/PESGM.2012.6345018.

[58] Unamuno E, Barrena JA. Hybrid ac/dc microgrids - Part I: Review and classification of topologies. Renew Sustain Energy Rev 2015;52:1251–9. https://doi.org/10.1016/j.rser.2015.07.194.

[59] Unamuno E, Barrena JA. Hybrid ac/dc microgrids - Part II: Review and classification of control strategies. Renew Sustain Energy Rev 2015;52:1123–34. https://doi.org/10.1016/j.rser.2015.07.186.

[60] Roggia L, Rech C, Schuch L, Baggio JE, Hey HL, Pinheiro JR. Design of a sustainable residential microgrid system including PHEV and energy storage device. Proc. 2011 14th Eur. Conf. Power Electron. Appl. EPE 2011, 2011.

[61] Dugan R. The Open Distribution System Simulator(OpenDSS). Sourceforge 2020:1–218.

[62] Southern California Edison. Southern California Edison DRPEP 2019.

[63] American wire gauge n.d. https://en.wikipedia.org/wiki/American_wire_gauge#cite_note-resperlength-11.

[64] California Energy Commission, NREL. CEC EVI-Pro 2019.

[65] NREL, CEC, Bedir A, Crisostomo N, Allen J, Wood E, et al. California Plug-In Electric Vehicle Infrastructure Projections: 2017-2025. 2018. https://doi.org/CEC-600-2018-001.

[66] State of California D of F. P-2: County Population Projections (2010-2060) 2019.

[67] Point 2 Homes. Oak View - Newland Population & Demographics 2019.

[68] Energy and Environmental Economics I (E3). RESOLVE: Renewable Energy Solutions Model n.d. https://www.ethree.com/tools/resolve-renewable-energy-solutions-model/.

[69] Kontar R El, Polly B, Charan T. URBANopt: An Open-source Software Development Kit for Community and Urban District Energy Modeling. 2020 Build Perform Anal Conf SimBuild 2020:293–301.

[70] National Fire Protection Association. 1965 NFPA Advance Report Volume 2. Poult Sci 1965;54:2138. https://doi.org/10.3382/ps.0542138b.

Appendix

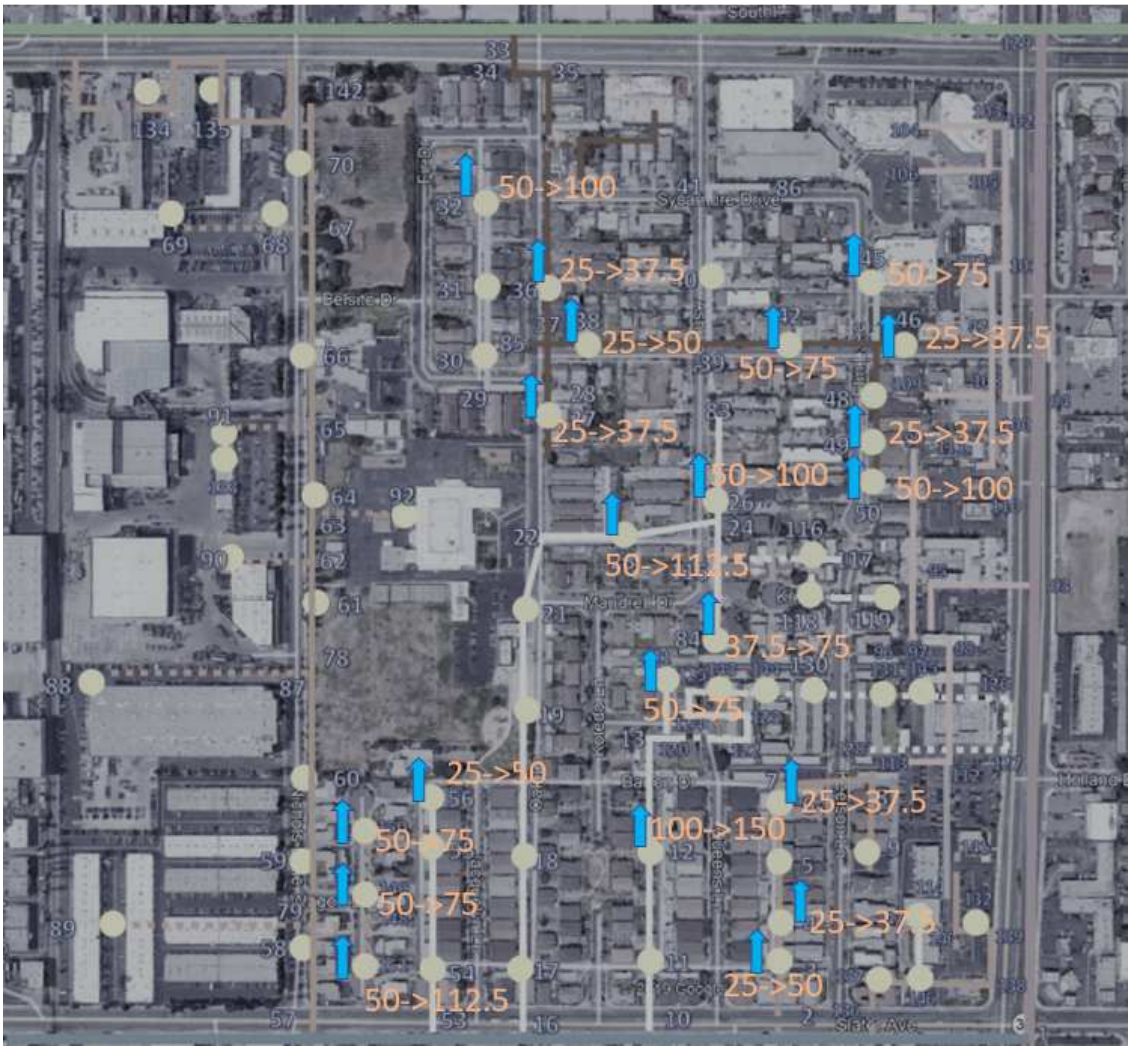

Transformer rating revision with URNANOPT Baseline

Revised Baseline transformer ratings used in OpenDSS Model:

Node number	Transformer Rating (kVa)	Node number	Transformer Rating (kVa)	Node number	Transformer Rating (kVa)
137	75	119	50	147	50
3	25	54	37.5	58	150
4	25	55	25	89	150
5	50	56	25	59	150
6	25	151	50	60	75
9	75	149	50	88	1500
11	50	150	50	61	25
12	50	36	25	90	150

121	50	27	25	64	100
143	100	30	100	92	300
144	100	31	50	91	50
130	50	32	50	133	350
131&145	150	38	25	66	75
17	50	40	100	68	50
18	100	42	50	69	150
19	25	45	50	n/a	25
21	112.5	48	25	135	300
23	50	49	25	134	25
84	37.5	50	50	35	300
26	50	46	25	152	150
116	50	n/a	112.5		
118	50	146	50		